Afifi M, Tremblay R, Rogers CA (2023), "Design and detailing recommendations of slotted-hidden-gap (SHG) connection for square HSS brace members", ASCE Journal of Structural Engineering 149(2): 04022249.

# Design and Detailing Recommendations of Slotted-Hidden-Gap (SHG) Connection for Square HSS Brace Members

Mohamed Afifi[1], Robert Tremblay[2], Colin A. Rogers[3]

[1] Lecturer, Department of Civil Engineering, McGill University, Montréal, QC, Canada. Email: mohamed.afifi@mail.mcgill.ca

[2] Professor, Department of Civil, Geological and Mining Engineering, Polytechnique Montréal, Montréal, QC, Canada. Email: robert.tremblay@polymtl.ca

[3] Corresponding author
Professor, Department of Civil Engineering, McGill University, Montréal, QC, Canada.
Email: colin.rogers@mcgill.ca
817 Sherbrooke Street West
Montreal QC, Canada, H3A 0C3
Tel. 514 398-6449

## ABSTRACT

The Slotted-Hidden-Gap (SHG) connection eliminates the need to reinforce the slot region of HSS braces of concentrically braced frames (CBFs). However, the existing design approach for SHG connections is rather empirical and limited by the range of the connection geometries and materials that had previously been tested. A general design approach based on the findings of a large-scale parametric study is presented in this paper, where the most critical parameters of the connection were varied. Different weld configurations were investigated to examine the effect of shear lag on the overall performance of the brace. The inelastic performance of SHG connected braces designed using the proposed approach was validated by means of numerically simulating the resulting braces and connections, and subjecting them to a reversed cyclic loading protocol. The simulated braces were able to attain their yield tensile resistance and fracture away from the connection region, while sustaining an axial deformation corresponding to an average storey drift of 5.43%. The proposed design and detailing method was, as such, found to be effective in the design of square HSS SHG connection braces ranging in size and steel grade.

**Keywords:** steel braces, HSS, welded connections, numerical modeling, design method.

## Introduction and Background

Hollow structural sections (HSS) are commonly selected as the bracing members for concentrically braced frames (CBF) due to their superior axial, flexural and torsional capacities, in addition to their aesthetic features favoured by architects. Braces form the principal factor affecting the seismic drift capacity of a CBF as they undergo alternating cycles of yielding in tension and buckling in compression. Thus, the braces must be designed to endure large inelastic deformations without major losses in strength and stiffness (Sabelli et al.,2013). According to capacity design requirements, the braces in a CBF act as the energy dissipating fuse of the seismic system where plastic deformations are assumed to concentrate. This strategy allows structures to survive design level earthquakes without losing their ability to carry post-earthquake gravity loads, given that the columns and beams are left for the most part undamaged (Sabelli et al.,2013). As part of capacity-based design, the brace connections must be protected by designing and detailing them to carry the probable (expected) resistance of the brace, which under tension excursions is anticipated to attain a force corresponding to the gross cross section yielding of the HSS brace member.

In a CBF system, HSS braces are connected to the beam-to-column joints in a bracing-bent of the frame through multiple configurations. The most widely used is the knife-plate welded connection, herein referred to as a conventional connection (Fig. 1a), in which slot cuts are created at the ends of the HSS braces where the plates are then inserted and attached using fillet welds. This connection detail, although vastly preferred due to its simplicity in design and fabrication, suffers major disadvantages; i.e. the reduced net section of the HSS brace due to the slots (Fig. 1b), and the uneven tensile stress distribution due to the shear lag effects. These drawbacks, in addition to the historical conservatism of shear lag factors (Cheng et al. 1998) (Willibald et al.,2006) (Zhao et al.,2008), have often challenged engineers to fulfill the capacity design requirements. The

Canadian Standards Association (CSA) S16:19 Cl.27.1.2 (CSA, 2019), the American Institute of Steel Construction (AISC) 341 Section B2 (ANSI, 2016), Eurocode 8 cl. 5.2.3.3 (EN 1998) and the Standard for design of steel structures of the People's Republic of China cl. 17.2.3 (GB, 2017) all include capacity design. To ensure that the brace dissipates energy during a seismic event, connections must have a factored resistance that surpasses the probable resistance of the brace. Inelastic behaviour is limited to the braces, while other parts of the SFRS (beams and columns, foundations, etc.) must remain essentially elastic to maintain structural integrity. To overcome this obstacle, various connection reinforcement schemes have been implemented by connection engineers, e.g., side-reinforcement plates (Fig. 1c) and wrapped-around welds (Fig. 1d). Both arrangements have undergone extensive research programs and have been demonstrated to be either uneconomic or unsuitable (Cheng et al. 1998) (Willibald et al.,2006) (Zhao et al.,2008) (Yang and Mahin, 2005) (Fell et al., 2006) (Haddad and Tremblay, 2006) (Martinez-Saucedo et al., 2006). The design formulations presented in this paper were derived for use with the Canadian CSA S16 Standard, however similar methodology could equally be followed using equivalent sections of other international codes & standards.

The slotted-hidden-gap (SHG) connection (Fig. 1e-f) represents an alternative to the conventional connection given that it eliminates the need for reinforcement of the brace ends. The SHG connection constitutes the creation of a slot cut into the plate, which is inserted into the slot in the HSS. This allows both the plate and the fillet welds to extend past the end of the slot in the HSS to the tube's gross cross-sectional area. After the assembly of parts, a gap is left between the end of the slot in the plate and the end of the slot in the HSS that is not visible once welding has been completed. The SHG was first introduced as the "extended plate configuration" in 1985 by Mitsui et al. (1985) after investigating several methods to repair the over-slot region of the conventional

connection. Their findings led to the first design recommendations of the extended plate configuration for circular hollow sections (CHS) published by the Architectural Institute of Japan in 2002 (AIJ, 2002). Between 2006 and 2008 Martinez-Saucedo et al. examined the possibility of utilizing the extended plate configuration for seismic applications through numerical simulations and laboratory testing of two circular hollow section (CHS) braces with SHG connections subjected to reversed-cyclic loading (Martinez-Saucedo et al., 2006, 2008a and 2008b). In 2010 Packer et al. conducted reversed-cyclic testing of four CHS braces using the SHG connection (Packer et al., 2010), followed by Okazaki et al. in 2013, who conducted dynamic physical testing of a chevron CBF subjected to a series of strong earthquake ground motions with square HSS braces connected using SHG detailing (Okazaki et al., 2013). A research group at McGill University and Polytechnique Montreal conducted finite element analyses (FEA) and laboratory testing of square HSS braces with various conventional and SHG connection detailing (Afifi et al., 2019, 2021 and 2022) (Moreau et al., 2014). A summary of the investigations carried out on SHG connections with the main findings is listed in Table 1. These studies illustrated the superiority of the SHG over the conventional HSS brace connection, and its ability to distribute inelastic demands away from the over-slot area. A deeper understanding of the local strain behaviours of different SHG connection configurations was also achieved; however, general design and detailing rules had not yet been developed for SHG brace connections.

Following from the experimental and numerical studies performed on the SHG connection, a deeper understanding of the global and local behaviours was achieved. Afifi et al. performed a preliminary numerical parametric study as part of this ongoing investigation in order to decide on the scope of the laboratory test specimens (Afifi et al., 2021 and 2022). Although the results showed the effects of varying individual parameters on the overall performance of the brace

models, this initial study did not assess the effects of varying different elements simultaneously. To decide on the most important parameters to be varied, free body cuts through different locations of the brace were utilized. Figures 2a and 2b show the different cross sections at critical regions, cross sections B through D (Fig. 2b) ensure the smooth load transfer from the HSS to the plate through the fillet welds, if adequately designed and detailed.

In order to prevent net section fracture in the HSS at the end connections during the high force tension cycles (anticipated strengths) of a seismic event, the primary goal of this study was to offer design and detailing recommendations for SHG connections. The expected tension force in seismic design frequently necessitates that the engineer reinforces the HSS (conventional connection) to comply with the capacity design requirements (specifically net section fracture). Thus, the SHG connection was devised to resist the expected strength under tension loading, without having to reinforce the net section of the HSS brace. Due to overall buckling of the HSS, the forces under compression loading (expected strengths) were expected to be lower (Fig. 3a). Therefore, the compression loading of the SHG connection is not regarded as being critical. Hinging at the ends of the bracing was designed to occur in either the paddle plate or the gusset plate, not in the region of the HSS connection (Fig. 3b-e). If a correctly designed and detailed braced bay were to fail during a seismic event, it would happen at the mid-length hinge of the brace (post buckling) due to low cycle fatigue fracture.

It is important to note that the use of the SHG connection does not mitigate the well documented failure mechanisms of HSS braces under cyclic loading. Its sole purpose is to avoid reinforcing the HSS while meeting capacity design requirements. As such, net section fracture was the main concern to be addressed, and thus, a tension protocol was utilized in the parametric study. The SHG connection is constructed in a fabrication plant firstly by creating the slots in both the HSS

and the plate. The slotted plate is then inserted inside the HSS slot until the flaps overlap the gross area of the tube with a distance of at least ($L_{wg}$) or a maximum gap ($L_{gap}$) of 30mm is left between the slots in the tube and gusset plate. Fillet welds are then applied on the interfaces of the HSS and plate. The SHG connection is designed to be constructed in a fabrication plant and then delivered assembled to the construction site ready to be field bolted to the beam-column interface. Hence, to facilitate construction it was assumed that a bolted field connection from the paddle plate to the gusset plate would be used as illustrated in Fig. 3b-e, and welding of the SHG connection (HSS to paddle plate) would be carried out in a fabrication shop.

Presented herein are the results of this parametric study aiming to evaluate the crucial parameters (Fig. 4) that influence the connection behaviour. Based on these observations, recommendations were proposed for the seismic design and detailing of the SHG connection for square HSS brace members.

## Large-scale Parametric Study

### *Overview and Scope*

Parametric finite element (FE) simulations were conducted to expand upon the findings from the laboratory tests conducted by the authors (Afifi et al., 2021). In previous investigations, a limited number of square HSS brace sizes were numerically analysed; thus, a wider spectrum of sections needed to be included to investigate the scale effects. The size of the HSS is likely to influence the stress profile in the brace due to the shear lag effects, which have a direct impact on the performance of the connection. In this investigation fifteen different HSS sizes were examined ranging from HSS 406×406×22 to HSS 76×76×4.8. As illustrated in Figure 5, each HSS size was modelled with two weld configurations, ten weld overlap lengths ($L_{wg}$), five plate thicknesses ($t_g$)

and five weld sizes ($D_w$) (Fig. 4). To minimize computations, the gap length ($L_{gap}$), defined as the hidden distance between the plate slot and HSS slot, was kept constant at the 30mm distance recommended by Martinez-Saucedo (2007). The gap length, although believed to be influential, was not investigated not only to minimize computations, but also due to the sufficiency of the current 30mm gap to meet the fabrication tolerances found in common practice. Material properties were kept constant for ASTM A1085 grade steel (ASTM, 2015) obtained from the testing program by Afifi et al. (2022). The ASTM A1085 steel grade has stricter rules on material properties with a minimum yield strength of 345MPa (50 ksi) and a minimum ultimate strength of 450 MPa (65 ksi) for all shapes. The expected material properties of the HSS ($R_yF_y$=1.25×345=431MPa) were comparable to the measured properties obtained from the coupon tests at $F_y$ = 434.3MPa (Afifi et al. 2022). The chosen steel grade resembles the Canadian HSS grade CSA G40.20. The objective is to design HSS connections for seismic applications, and thus ASTM A1085 grade was the main focus of this study. ASTM A500 was not considered in the study, as both ASTM A1085 and CSA G40.20 impose stricter rules on the limits of yield and ultimate capacities. The study comprised 7,500 FE models, which is the number of all possible combinations of the parameters shown in Fig. 5.

The parameters chosen for examination in the parametric study were found to be the most influential during prior phases of this study (Afifi et al., 2019, 2020, 2021, 2022), and thus were selected to be further investigated. The ranges shown in Fig. 5 were selected to fulfill the capacity-based design requirements for HSS braces, and reflect the sizes found in practice. The weld dimensions (size and length) were selected to insure adequacy with respect to base-metal fracture, as well as weld-metal fracture. The increments of increasing the weld size were of ¼" (6 mm), typical of what is found in fabrication practice in North America. The thicknesses of the plate were

selected to make sure that failure in tension cycles did not occur in the plate itself (i.e., yielding), and to investigate how the enlarged thickness of the plate affects the performance of the SHG connection. The range for each parameter was chosen to provide a representative sample size while optimizing needed computational time and cost.

### *Methodology*

The FE models were developed in the commercial software ABAQUS-6.14-2 (Dassault Systems, 2014). A set of what is herein referred to as base models was created in AutoCAD 2019 (Autodesk, 2019). These models were then imported into Abaqus, where the appropriate meshing and element material properties were applied. There was a total of thirty base models; i.e. fifteen HSS sizes with the two weld configurations A and B as featured in Table 2. Weld configuration B utilizes an equivalent longer length smaller sized weld as compared to configuration A.

After creating the base models their input files (.inp) were generated using Python (Lutz, 1996) scripting, nodal coordinates of different elements of the connection were parametrized, or in other words given variable designations instead of unique discrete values. To insure integrity, geometric relations between elements of the connection were respected through introducing shape constraints. Afterwards, a script file (.psf) was created containing Python instructions to generate designs, execute simulations, and gather outputs for the parametric variations of the parametrized input file (MIT, 2017). A displacement loading was applied at the plate end, while the reaction forces were measured at the other end of the HSS. As mentioned previously, the main objective of the paper is to investigate the net-section failure occurring at the connection and how to detail SHG connections in order to force fracture away from the connection region, hence a tension protocol

was utilized in the parametric study. Global behaviour was assessed primarily through the overall load-displacement response, and local behaviours were assessed through the values of von Mises stresses ($S_{Mises}$) and equivalent plastic strains (PEEQ) at critical points in the different connection elements. The vertical displacement (U2) was also evaluated at the plate to assess the bowing effect. A summary of the main evaluation points is shown in Figure 6.

*FE Modelling Environment*

The properties of the FE models were described in detail in previous publications (Afifi et al., 2021 and 2022); only the highlights are contained herein. One-quarter of the square HSS tube was modelled with appropriate symmetry and loading boundary conditions (Fig. 7). A sensitivity analysis was done to ensure that the one-quarter model with symmetry indeed provides comparable results to the full model. To avoid having differing gauge lengths, as discussed in Afifi et al. (2022), the distance between the slot in the HSS and the mid-length of the brace was kept constant regardless of the overall brace length. The main features of the models were chosen to be representative of those seen in the laboratory experiments; including boundary conditions, geometry, material properties, and the imposed loading protocol (Afifi et al., 2019, 2021 and 2022).

Mesh sensitivity analysis was performed for each of the thirty base models before proceeding with varying the parameters. To ensure that the chosen densities of the mesh will indeed cover the entire range, another mesh sensitivity analysis was run on models with the largest dimensions of elements (largest plate thickness, largest weld size, etc.), in which the mesh densities were further refined to insure consistency throughout the different simulations. Stepping at the end of the weld was mimicked through the slanted edges of the modelled weld shape (Fig. 8c). Coupon data from

the tests described in Afifi et al. (2022) was used to obtain the true stress-strain curves for different components of the connection. The true stress-strain curves were later imported into the software as material properties of the HSS and plate. The true stress-strain curves for welds are difficult to obtain, thus the measured material properties from the HSS flats were used instead. The effects of the modified stress-strain properties in the corners of the HSS and longitudinal residual stress distribution profile were incorporated in the FE models as per the findings of Koval (2018). A non-linear isotropic von-Misses hardening module was used to model all materials. The main features of the FE models can be seen in Figure 8.

***Comparison of numerical and experimental results***

A calibration study was performed with the objective of validating the FEMs before conducting the full parametric study. The experimental programs conducted by Moreau et al. (2014) and Afifi et al. (2022), and the numerical studies performed by Martinez-Saucedo et al. (2006) and Afifi et al. (2019, 2021 and 2022), were selected as a starting point for this calibration study because these studies comprised several SHG connections setups and different HSS sizes and grades, hence allowing for better confidence in the modelling technique and results. As an example, the predictions of the FE model are found in Figure 9, along with the experimental measurements, for an HSS 254×254×13 with weld overlap length ($L_{wg}$) of 20mm (Fig. 9a) and 0mm (Fig. 9b) (bolted paddle-gusset plate connection as per Fig. 3c). The FE model predicted accurately the connection response under a monotonic tension loading protocol. The location of the fracture was also accurately predicted for the SHG connections with different overlap lengths, whether at the mid-length for the $L_{wg}$=20mm specimen or at the lower connection as seen in the specimen with $L_{wg}$=0mm.

## Results and Discussion

### *Overall load-displacement response*

The normalised overall load-displacement response for the SHG connection brace models of different HSS sections and having different weld overlap lengths ($L_{wg}$) is provided in Figure 10; all other parameters were kept at their control values. Although damage was not modelled, a code function was added to Abaqus to "kill" the elements when the equivalent plastic strain (PEEQ) reached a critical fracture value of 1.0. Failure PEEQ was obtained through FE models calibrated against physical testing specimens as presented in Fig. 8. The obtained failure PEEQ value was in agreement with the range proposed by Zhao et al. (2008). This approach is also known as the element death feature, a similar methodology was implemented in Martinez-Saucedo et al. (2007) and Afifi et al. (2022).

All HSS sizes showed a similar overall response of sharing the same initial elastic stiffness before attaining the yield resistance ($P/P_y$=1.0), where $P_y = A_g F_y$, on the gross area of the HSS. The SHG brace models without a weld extension beyond the HSS slot ($L_{wg}$=0mm) fractured prematurely at the over slot region. Gradually extending the weld overlap length showed slight improvement in ductility by delaying the failure displacement, despite fracturing at the net section, until a point beyond which the brace was able to attain its full ductility and fracture in the gross area of the tube and away from the connection region. Extending the weld overlap length past this value did not grant the brace any additional ductility, although slightly decreased the stress levels in the HSS tube. A sample of the Abaqus results of HSS203×203×13 is shown in Figure 11. A weld overlap length below 20mm caused fracture in the net section area, and weld overlap lengths of 20mm or more forced inelastic demands away from the connection and helped the brace to attain its full yielding

capacity, with fracture occurring at the mid-length. The weld overlap length value at which each HSS was able to reach its full capacity was noted as the minimum required overlap length, and was further investigated to understand the significance behind this value.

The results shown in Figures 10 and 11 are of models with weld configuration A. A similar response was obtained from the models with weld configuration B. A summary of the minimum weld overlap length ($L_{wg,\,min}$) along with other ratios is given in Tables 3 and 4.

To further explore the identified minimum overlap weld length and to normalize the results from the several HSS sizes, various ratios of weld overlap lengths to other parameters were calculated. Despite the changing weld configurations, a similar specified overlap length was chosen. For example, the HSS 406×406×22 has a specified overlap length of 40mm for both configuration A ($L_w$=610mm, $D_w$=38mm) and configuration B ($L_w$=920mm, $D_w$=25mm). The obtained minimum weld overlap ratio ($L_{wg}/L_w$) challenges the 5% limit obtained previously in Moreau et al. (2014) and Afifi et al. (2022). Although the average of the minimum weld overlap ratio was 4.5% for weld configuration B models (Table 4), the minimum average ratio came in at 7.3% for weld configuration A models (Table 3). This can be attributed to the stiffer nature of the FE models compared to the physical testing specimens, as well as the material and geometric discrepancies. The ratio of the overlap length to the width of the HSS slot ($L_{wg}/t_{slot}$) needed to be explored based on the recommendations of Moreau et al. (2014) and Afifi et al. (2022). Values of $L_{wg}/t_{slot}$ ranged from 0.91 to 0.69 for both weld configurations with averages of 0.76 and 0.85 for configuration A and B, respectively. A new ratio $X_v$ is introduced herein (Eq. 1).

$$X_v = \frac{Lwg/t_{slot}}{Ane/Ag} \tag{1}$$

The value $X_v$ is the quotient of ratios ($L_{wg}/t_{slot}$) and ($A_{ne}/A_g$). The advantage of this ratio is that it takes into consideration the shear lag factor (U) incorporated in the calculation of the effective net area $A_{ne}$. The values of $X_v$ ranged from 1.11 to 0.82 for configuration A, and from 1.14 to 0.77 for configuration B. The ratio $X_v$ is believed to be a key parameter in controlling the response of the SHG connection.

***Local strain behaviour***

A closer look needed to be taken at the minimum overlap length for each HSS size and weld configuration. Local plastic strains (PEEQ) were evaluated at different points along the HSS starting at the slot and ending at the mid-length (Fig. 6). The variation of PEEQ response along the HSS at failure is shown in Figure 12. For this analysis, the HSS size, weld configuration and weld overlap length, as well as the thickness of the plate, were varied. To normalize the findings from these simulations, the ratio $X_v$ was used.

The numerical models with no weld overlap ($L_{wg}$=0mm and $X_v$=0.0) reached a failure PEEQ value of 1.0 at the slot, which rapidly decreased over the adjacent three evaluation points (S+3). From this point on, a PEEQ of approximately 0.2 was maintained up to the mid-length. These models were not capable of distributing plastic strains along the full length of the HSS; instead, the strain demand was concentrated at the connection, where failure eventually occurred. A gradual increase in $L_{wg,}$ and accordingly the value of $X_{v,}$ showed a steady decrease of the inelastic strain values at the slot with a corresponding increase along the HSS length. The PEEQ value at the mid-length surpassed the PEEQ at the slot for the first time at $X_v$=1.0. This is potentially an indicator of the minimum weld overlap length ($L_{wg}$) sufficient to develop the full yielding capacity of the HSS at the gross area, and to prevent premature fracture at the net section. At $X_v$=2.0 the brace models

showed the mirrored response of $X_v$=0.0; the failure PEEQ value occurred at the mid-length. This indicates that failure is most certainly to occur at the mid-length away from the over slot region. Extending the weld overlap length beyond $X_v$ of 2.0 did not show any further change in the strain behaviour.

The PEEQ values at failure vs. $X_v$ at the slot and the mid-length have been provided in Figures 13a and 13b, respectively. The bar and whisker plot provides a five-number summary as follows: the minimum, first quartile, median, third quartile, and the maximum. The whiskers go from each quartile to the minimum or maximum and vertical line goes through the box at the median. The results illustrate the principal changes in inelastic demand concentrations at the slot region and the mid-length. This observation highlights prior findings of shifting the inelastic demands from the slot region to the mid-length at the unity value of $X_v$. The variability in PEEQ results at each $X_v$ point come as a result of increasing the weld side ($D_w$).

To better display the effect of varying all the parameters, a 3D surface plot is provided in Figure 14. The HSS slot (Fig. 6) was deemed the most critical evaluation point at which to assess the inelastic demands. The variations in HSS size, weld overlap length ($L_{wg}$), weld length ($L_w$), and plate thickness ($t_g$) are incorporated in the $X_v$ ratio. The increase in weld size ($D_w$) was plotted in descending order.

Weld size, $D_w$, was increased in increments of 6.4mm (¼”) to match the commercially specified weld sizes. At $X_v$=0.0, increasing the weld size by 25.4 mm (1”) has decreased the PEEQ value at the slot from 0.99 to 0.88, and similarly at each $X_v$ value until $X_v$=2.0. Beyond this value of $X_v$ enlarging the weld did not have an effective impact on the inelastic demand at the slot. This suggests that although increasing the weld size ($D_w$) might relax the inelastic demands and lower

their value at the HSS slot, this change is not sufficient on its own to shift the location of the fracture from the net section to the mid-length of the brace.

***Free body cuts- Capacity of weld overlap length***

Free body cuts were used as a method to examine the different force transfer mechanisms in the conventional and SHG connections in Afifi et al. (2021). The load participation factor, or the percentage of the load carried by each of the elements of the connection, at different locations was obtained and highlighted (Fig. 15a). The maximum load participation factor of the fillet weld, the focus of this analysis, for weld configurations A and B is provided in Figures 15b and 15c in comparison with $X_v$. Both weld configurations showed similar response; the weld force participation percentage increased uniformly with an extension of the weld overlap length until an $X_v$ ratio of 1.5. Beyond this point, the increase in weld overlap length did not significantly augment the weld load participation. Although similar weld overlap length was required for a certain HSS size under both weld configurations, as suggested in Tables 3 and 4, the load participation factor of the welds at each configuration was different. The values highlighted by the stars are 19.4% for configuration A and 11.1% for configuration B (Fig. 15b&c). The highlighted numbers are the target value for which if the weld overlap length is adequately designed and detailed will be sufficient to develop the full capacity of the brace. Each of the modelled HSS sizes with the corresponding capacities at yielding on the gross area of the section ($T_y = A_g F_y$) and fracture of the net section ($T_r = A_{ne} F_u$) are listed in Table 5 for both weld configurations. The formula $1-(T_r/T_y)$ represents the loss in HSS capacity at the net section as a percentage of the yielding strength ($A_g F_y$).

Due to the reduced shear lag effects for models with longer welds (Configuration B), the effective net area ($A_{ne}$) was larger, and consequently the difference between the net section fracture and yielding of the gross area was lower compared to the models with shorter welds (Configuration A). On average, the reduction in capacity at the net section, as a percentage of the gross yielding strength, was 18.1% for configuration A and 10.4% for configuration B. These percentages come in close agreement with the maximum weld participation factors highlighted in Figure 13; 19.4% and 11.1% for configurations A and B, respectively. This similarity suggests that the length of the weld overlap ($L_{wg}$) must be chosen to account for the difference between the gross cross-section yielding resistance and the net section fracture (accounting for shear lag) in order to develop the full ductility of the HSS and to prevent premature failure at the over slot region. To verify this approach, a single-variable regression analysis was carried out between the weld participation factor for each model and the corresponding 1-($T_r/T_y$) formula and values were in agreement with R-squared value of 0.946 and a root mean square error (RMSE) of 0.212.

***Paddle Plate Behaviour***

In the SHG connections, the eccentricity of the tension force transferred from the weld to the paddle plate causes in-plane flexural demand in the plate. This phenomenon is referred to as plate rotation or bowing effect (Martinez-Saucedo, 2007) (Afifi et al., 2021). A 3D surface is provided in Figure 16 showing the relation between the vertical displacement ($U_2$) at the plate flap (Fig. 6) and the plate thickness ($t_g$) and overlap length ($L_{wg}$) for the largest modelled brace section (HSS 406×406×22). Plate rotation increased with the larger weld overlap length ($L_{wg}$) and decreased while enlarging the plate thickness ($t_g$). Plate rotation appears to be function of the location of the weld start, the load carried by the weld, as well the moment of inertia (I) of the plate flap. Hence, the depth of the plate flap (Fig. 4) must be dimensioned to effectively limit this bowing effect.

## Proposed Design Method

The following design methodology was formulated following specific clauses in CSA S16:19 (2019), however this methodology could equally be followed using equivalent sections of other international codes & standards (e.g. AISC 360 (ANSI 2016) & AISC 341 (ANSI 2016)). The flow of a proposed design method for the SHG connections of HSS braces is shown in Figure 17. The design of the connections involves selecting a minimum practical weld length ($L_w$) to avoid block-shear fracture at the connection. The remaining components of the connections (Fig. 4) such as the plate width ($W_g$) and thickness ($t_g$), as well as weld size ($D_w$) are selected based on this weld length ($L_w$). It is important to follow the suggested design flow, meaning that if at any point a certain dimension needs to be altered, one must revisit the other dimensions based on the new modification.

The probable brace resistance in tension (Cl. 27.5.3.4 of CSA S16-19) is given by Equation 2, where $A_g$ is the gross cross-sectional area of the HSS brace and $R_yF_y$ is the probable yield strength specified in Clause 27.1.7 of CSA S16-19 for HSS members (CSA, 2019).

$$T_{prob} = A_g R_y F_y \tag{2}$$

The minimum weld length for each HSS size is selected based on the limit state of block-shear fracture occurring in the tube at the connection. The block shear design in the context of the current Canadian CSA S16-19 standard (CSA, 2019) is given by C1.13.11 (Eq. 3). In carrying out the capacity design check, Eq. 3 can be modified by replacing $\phi_u$ with 1.0, and substituting $F_y$ and $F_u$ with their probable stress values depending on the tube grade and specification (Eq. 3a). To obtain a simplified version of the block shear equation, the tensile component can be ignored, given the small net area $A_n$ associated with this specific connection configuration; the shear component of

the equation, alone, is considered. To further simplify it, the ultimate probable tensile resistance can be used instead of the average of probable yield and ultimate resistances as recommended by (Willibald et al., 2006). The total area in shear, $A_{gv}$, is given by $4L_{wt}t_{HSS}$. Finally, Equation 3b can be rearranged so that $L_w$ is the subject of the formula, and by replacing $T_r$ with $T_{prob}$ (Eq. 3c). A resistance factor $\phi$ of 0.90 is used as currently specified in CSA S16:19.

$$T_r = \phi_u \left[ U_t A_n F_u + 0.60 A_{gv} \left( \frac{F_y + F_u}{2} \right) \right] \tag{3}$$

$$T_r = \left[ U_t A_n R_t F_u + 0.60 A_{gv} \left( \frac{R_y F_y + R_t F_u}{2} \right) \right] \tag{3a}$$

$$T_r = 0.60 A_{gv} R_t F_u \tag{3b}$$

$$L_w = \frac{A_g R_y F_y}{\phi \; 0.60 \; (4 t_{HSS}) R_t F_u} \tag{3c}$$

After obtaining the weld length, the plate width, $W_g$, is calculated using Equation 4 obtained through computing Plate Yielding on the Whitmore Area (Cl. 13.2 CSA S16-19), where B is the depth of the brace section.

$$W_g = 2 L_w \tan 30° + B \tag{4}$$

Consequently, the plate thickness, $t_g$, can be computed using Equation 5.

$$t_g = \frac{A_g R_y F_y}{\phi \; W_g F_{y,gusset}} \tag{5}$$

Using the plate width and thickness, a check of block shear fracture in the plate needs to be carried out using Equation 6. Equation 3 is used with the following substitutions: $U_t = 1.0$ for symmetrical

block failure, $A_n = Bt_g$ and $A_{gv} = 2L_wt_g$. Notice that the yield and ultimate strengths in Equation 6 are of the paddle plate. A resistance factor $\phi_u$ of 0.75 is used as currently specified in CSA S16:19.

$$T_r = \phi_u \left[ Bt_g F_u + 0.60(2L_w t_g) \left( \frac{F_y + F_u}{2} \right) \right] \quad (6)$$

The fillet weld size, $D_w$, is computed based on the limit states of base-metal fracture (Cl. 13.13.2.2 CSA S16-19) occurring at the weld-to-HSS by using Equation 7a, where $F_u$ is the ultimate nominal stress of the HSS (CSA, 2019). Base-metal fracture of the weld-to-plate interface is checked using the same equation, but with using the ultimate nominal stress of the plate for the value of $F_u$ and $\phi_w$ of 0.67.

$$V_r = 0.67\ \phi_w A_w F_u \quad (7)$$

$$V_r = 0.67\ \phi_w (4L_w D_w) F_u \quad (7a)$$

Weld metal fracture (Cl. 13.13.2.2 CSA S16-19) is also checked through Equation 8 to insure sufficient resistance of weld metal (CSA, 2019). Equation 8a can be derived by assigning $A_w$ with the area of the effective weld throat, setting the angle θ between the weld and loading orientation to 0°, $M_w = 1$ for welds all oriented in the same direction, and $\phi_w$ of 0.67. $X_u$ is the ultimate tensile strength of the electrode.

$$V_r = 0.67\ \phi_w A_w X_u (1.00 + 0.5 \sin^{1.5} \theta) M_w \quad (8)$$

$$V_r = 0.67\ \phi_w (4L_w\ 0.707 D_w) X_u \quad (8a)$$

***Minimum weld overlap length ($L_{wg}$):***

As per the findings of the parametric study, the weld overlap length, $L_{wg}$, is proposed to be computed through two main approaches. The first approach deems the overlap length to be

sufficient when the $X_v$ ratio (Eq. 1) is equal to or greater than 1.0. Rearranging the equation so that $L_{wg}$ is the subject of the formula yields Equation 9:

$$L_{wg} \geq \frac{A_{ne}}{A_g} t_{slot} \quad \text{while } \frac{A_{ne}}{A_g} \geq 0.7 \tag{9}$$

Where $A_g$ is the gross area of the HSS, and $t_{slot}$ is the width of the slot in the HSS, which is typically 3mm wider than the thickness of the paddle plate ($t_g$ +3mm) based on standard detailing protocols. A limit of $A_{ne} \geq 70\% A_g$ is considered to prevent extending the weld overlap to unrealistically long lengths. $A_{ne}$ is the effective net area of the tube accounting for shear lag (Eq. 10). Equation 10a shows the net area, $A_n$, as function of the gross area, $A_g$, width of slot, $t_{slot}$, and thickness of HSS, $t_{HSS}$.

$$A_{ne} = UA_n \tag{10}$$

$$A_{ne} = U\left(A_g - 2(t_{slot}t_{HSS})\right) \tag{10a}$$

Where U is the shear lag factor (Cl. CSA S16-19) calculated as follows:

$$U = 1.0 \text{ for } \frac{\overline{X'}}{L_w} \leq 0.1 \qquad \text{or} \qquad 1.1 - \frac{\overline{X'}}{L_w} \text{ for } \frac{\overline{X'}}{L_w} > 0.1 \tag{11}$$

Where $L_w$ is the weld length and $\overline{X'}$ is the distance between the centre of gravity of one-half of the HSS cross section taken from the edge of the paddle plate (Fig. 18).

The second approach, whose need was demonstrated by means of analysing the force transfer in the connection using free body cuts (Fig. 15), mandates extending the weld overlap length so that it is sufficient to resist in shear the difference between the probable gross area yielding ($T_{prob}$) and

net section fracture resistance of the HSS ($T_r$). The partial safety factor, $\phi$, of 0.9 was implemented to account for weld irregularities.

$$L_{wg} \geq \frac{T_{prob} - T_r}{\phi\ 0.67\ (4D_w)\ F_u} \tag{12}$$

where

$$T_r = UA_nF_u \tag{13}$$

It is recommended that the weld overlap length be taken as the maximum value of the two approaches (Equations 9 and 12).

***Minimum depth of plate flap ($d_{flap}$):***

To minimize the bowing effect in the flaps of the paddle plate, which was demonstrated to worsen with increased weld overlap length, the plate flaps should be adequately dimensioned to minimize those rotations. Moreover, an excessively rotated paddle plate places extra plastic demand at the connection at the weld ends leading to possible premature fracture. Figure 19 is a schematic of the plate rotations along with the idealized model of a cantilever beam. Free body cuts have revealed that the fillet welds are responsible for the transfer of force from the HSS to the plate. This load transfer happens over a short segment of weld, near the tip of the plate, and hence the load carried by the weld overlap length can be applied as a point load on the cantilevered flaps of the paddle plate.

The maximum deflection of a fixed end cantilever beam is given by:

$$\delta_{max} = \frac{PL^3}{3\mathrm{EI}} \tag{14}$$

The cantilevered length in the slotted paddle plate, L, is the summation of the weld overlap length and the gap length ($L_{wg}$+ $L_{gap}$). Half of the transfer force will be applied to each plate flap, where the force is taken as the difference in values between the net section fracture ($T_u$) and gross area yielding ($T_y$). The moment of inertia of the plate flap is defined as:

$$I = \frac{t_g d_{flap}^3}{12} \tag{15}$$

To verify this approach, a linear regression analysis was carried out between the in-plane vertical displacement ($U_2$) values obtained from FE analysis and those calculated with Equation 14. The deflection values were in agreement, resulting in an R-squared value of 0.946 and a root mean square error (RMSE) of 0.285. As the shape of the plate is sloped, a variable moment of inertia I(x) could have been used, but for reasons of conservatism and simplicity, the least depth was chosen to be utilized in the calculation of I (Eq. 15). Equation 16 is obtained through setting Equation 14 equal to the least conservative deflection limit of L/180 for cantilever beams, which could be replaced by a more conservative figure if so desired. Note, for the largest HSS braces included in the parametric study, this L/180 limit equates to only 0.45 mm. The proposed limit diminishes the plastic demand at the connection that can occur as a result of the in-plane plate rotation. As seen from the results of the analyses, problematic deformations of this portion of the plate did not occur, and hence the L/180 limit was considered appropriate for design. Arranging the formula to make $d_{flap}$ the subject results in:

$$d_{flap} \geq \sqrt[3]{\frac{12\left(\frac{P}{2}\right)\left(L_{gap}+L_{wg}\right)^3}{3\,E\,tg}} \tag{16}$$

***SHG Detailing:***

This Section describes the detailing aspects of the SHG connection that were considered when calculating the length of slot in the HSS, the length and width of the paddle plate slot, and the length of the hidden gap (Fig. 4).

The length of the plate inserted into the HSS, $L_g$, is calculated as the length of the weld, $L_w$, in addition to the tolerance length, $L_{tol}$. The tolerance length is the fabrication clearance left before the start and the end of the weld, and is usually assumed to be between 1 to 2 times the size of the weld, $D_w$. Accordingly, the length of the slot in the HSS, $L_{wn}$, is computed through subtracting the length of the weld overlap, $L_{wg}$, and the tolerance length, $L_{tol}$, from the total length of the plate slot, $L_g$. The width of the slot in the plate, $W_{gs}$, is taken to be the outer dimension of the HSS + 3 mm to account for typical fabrication tolerances, while the length of the slot in the plate, $L_{gs}$, is taken as the length of the overlap added to both the tolerance lengths and the gap length, $L_{gap}$. The length of the hidden gap was kept at the 30mm, as recommended by Martinez-Saucedo (2007). For seismic applications, a distance of $2t_g$ must be left in the paddle plate after the end of the plate insertion distance $L_g$, to force the flexural demands away from the HSS (Fig. 3b-e). Equations 17 to 19 detail the calculations of $L_g$, $L_{wn}$, and $L_{gs}$ respectively. The detailing variables are also illustrated in Figure 4.

$$L_g = L_w + 2L_{tol} \tag{17}$$

$$L_{wn} = L_g - L_{tol} - L_{wg} \tag{18}$$

$$L_{gs} = L_{wg} + L_{tol} + L_{gap} \tag{19}$$

## Validation of Recommended SHG Design Method

***Correlation between developed equations and simulated models***

As a first validation step, a regression analysis was carried out to observe the confidence level in the proposed guidelines against the historical testing and modelling results of SHG brace connections. A comparison of the weld overlap lengths calculated through the proposed methodology against the recommendations of the AIJ (2002) and Moreau et al. (2014) is shown in Table 6 and Figure 20.

Generally, variations between the three methodologies decreased as the HSS member became smaller. This is explained by the range of the HSS sizes tested in previous research programs. For the shorter length larger size welds (Config. A), the proposed equations showed to be more conservative than the 5% weld extension recommended by Moreau et al. (2014). However, both methodologies showed to be in better agreement while utilizing smaller sized longer length fillet welds (Config. B). This can be attributed to the stiffer nature of the FE models compared to the testing specimens. The AIJ methodology, which relies only on the thickness of the paddle plate, was found to be overly conservative, and accordingly the depth of the plate flap would need to be enlarged unnecessarily to reduce the rotations induced by the extended welds (AIJ, 2002). The proposed equations provide a reasonable alternative to the over conservatism of the AIJ guidelines (AIJ, 2002) and are either slightly conservative or in agreement with the extension of 5% of total weld length ($L_w$) beyond the HSS slot as recommended by Moreau et al. (2014) and Afifi et al. (2021).

***SHG Braces under reversed cyclic loading***

To further validate the proposed design and detailing methodology, three full braces and their SHG connections were designed following the steps outlined above. These braces and connections were then modelled numerically to evaluate the performance of the SHG connection when subjected to a reversed cyclic loading protocol. The intent for these models is to provide a “proof-of-concept” and

to show that the SHG connected braces designed with the proposed guidelines would attain drift ratios similar to those measured for HSS braces with conventional reinforced connections. The intent is to demonstrate that the brace and its end connections will sustain the tension loading, while remaining unaffected by the compression loading. Unlike for the monotonic tension models, quarter models with symmetry were not utilized. Instead, full FE models of the HSS brace and SHG connection were employed in the study when the reversed cyclic loading protocol was applied. This was done to capture the influence of the anticipated local and global imperfections on the response to loading, as well as the interaction of the connection components.

The long brace specimen from Moreau et al. (2014) and Afifi et al. (2021) was recreated in Abaqus. Global imperfections were simulated through conventional buckling analysis and were proportioned to the first buckling mode with a multiplier according to the recommended limits of manufacturing tolerances for HSS members (l/1000). Material plasticity was modeled with a combined half cycle hardening module with 10 backstresses. Material fracture was matched through the element death feature discussed in Afifi et al. (2022). Elements were deemed failed and thus killed when a critical ratio of equivalent plastic strain to the critical failure strain exceeded unity. The results of the calibrated model in comparison with the test run by Moreau et al. (2014) can be seen in Figure 21.

The length of the HSS was designed to represent actual brace lengths of typical CBFs in low-to-medium rise buildings detailed with a bolted paddle-gusset plate connection to minimize welding on-site (Fig. 3b-e). Multiple paddle-gusset connection scenarios were investigated in Afifi et al. (2019) and the 4-angles detail (Fig. 3c) was utilized in the experimental program by Afifi et al. (2022). The models were sized assuming that the brace is part of a 4-m high chevron frame and has an inclination angle of $\theta = 45°$ to the horizontal, the bay width of the frame is 8.5m. Assuming negligible brace elongation in the paddle-gusset plate connection, the axial deformations were

assumed to occur uniformly over the HSS length ($L_B$), and a factor was used to transform the deformations of the brace from its centre-to-centre dimension $L_{o-c}$ to its $L_B$ dimension (Fig. 22). The 1.3 transformation factor reported by Tremblay et. al. (2008) was revised to 1.4 because the paddle-gusset connection detailing is longer than attaching the HSS directly to the gusset at the beam-column connection of the CBF. Thus, equation 20 can be derived to relate the axial brace deformations in a frame to its interstorey drift. In the shown configuration, the hinge points were expected to take place $2t_g$ after the end of the angles. The $2_{tg}$ offset is critical as it forces the flexural demands away from the HSS and the connection region and allows the formation of the plastic hinge in the gusset plate.

$$\frac{\delta}{L_H} = 1.4\, sin\,\theta\, cos\,\theta \frac{\Delta}{h_s} \tag{20}$$

The numerical models were subjected to a protocol similar to that used for the testing of the long brace reported in Moreau et al. (2014) and Afifi et al. (2021). As can be seen in Figure 23, the protocol involved increasing symmetric displacement amplitudes until an IDR of 2.5%, after which two cycles per displacement excursion were applied to assess the residual strength and stiffness of the brace and, lastly the brace was displaced to higher amplitudes until failure. It was desirable to subject the connection to the maximum tensile displacement demands that may occur during an earthquake before damage localised at the mid-length plastic hinge region. Thus, the loading protocol consisted of two portions: a near-fault tension dominated protocol followed by a far-field symmetric protocol.

The geometric properties and probable resistances of the three braces modelled under reversed cyclic loading are given in Table 7. The sections were chosen to represent common HSS sizes utilized in construction of low-to-medium rise concentrically braced frames in Canada and the USA. The $b_{el}/t$ for the chosen sections ranged between 15.1 and 15.8 to meet the class requirements

of MD and LD systems (CSA, 2019). The response to loading of the three SHG HSS braces designed with the proposed guidelines were generally found to be similar. The normalised overall load-IDR response for SHG braces made of HSS 254×254×13 with $L_{wg}$=28mm as per the proposed recommendations are displayed in Figure 24. The SHG connection brace designed and detailed according to the proposed guidelines herein is found to be adequate to sustain the load reversals.

The difference in response as a result of the connection detailing can be clearly observed. The HSS brace model with SHG connection designed according to the proposed guidelines showed more ductility through undergoing approximately 23 cycles before experiencing local buckling and fracturing at the mid-length after attaining a maximum normalised load of 1.19 and an IDR of 5.61%. This is superior to the IDR of 5.0% reported for reinforced square HSS brace connections tested by Fell et. al. (2009) and exceeds the 5.4% average drift ratio reported by Yang and Mahin, (2005) and Fell et al. (2006) for unreinforced square HSS braces but with extending the weld length at least 1.56 times the circumferential distance between welds for one-half of the tube to diminish shear lag effects. On the contrary, the brace model of a conventional unreinforced connection fractured at the bottom connection during the $9^{th}$ cycle and the simulation stops at that point. The latter attained a maximum normalised load of 1.13 and a maximum IDR of only 1.76%.

## Conclusions & Recommendations

The main objective of this research project was to provide design and detailing methodology for the SHG connection for square HSS brace members for seismic applications. This objective was attained through a combination of laboratory testing and numerical modelling of various SHG connections. A large-scale parametric study was performed to determine the influence of different

parameters affecting the performance of SHG HSS brace connections. The major findings from these phases are:

- The HSS width B, HSS thickness $t_{HSS}$, plate thickness $t_g$, weld size $D_w$, weld length $L_w$, weld overlap length $L_{wg}$ and gap length $L_{gap}$ were found to be the geometric parameters that principally affect the performance of the SHG connection.
- For all HSS sizes, gradually extending the weld overlap length from 0mm showed slight improvement in ductility by delaying failure displacement, until a point beyond which the brace was able to attain its full ductility and fracture in the gross area of the tube and away from the connection region. This value was noted as a target minimum weld overlap length.
- A unity value of the ratio $X_v$ was found to be sufficient to limit inelastic demands at the connection region and force the brace to yield extensively on its gross area and fracture in the mid-length.
- Freebody cuts revealed the load participation factor of the fillet welds increased with an increased overlap length, until a point beyond which a plateau occurs and the load participation factor stays almost constant.
- The proposed design method is based on the maximum value obtained for the weld overlap length, which is obtained by either equating the $X_v$ ratio to one or by assuming that the weld overlap length resists in shear the balance between the net section fracture and gross area yielding of the brace.
- The depth of the plate flap is decided based on the assumption of an idealized cantilever deflection to limit the rotation of the plate as a result of the load transferred from the HSS to the plate through the fillet welds.

- The proposed equations for weld overlap length showed to be slightly conservative compared to the 5% weld length extension recommended previously. The equations are reasonable compared to the AIJ recommendations, which were shown to result in overly conservative designs with larger HSS sizes.
- The brace models designed and detailed with the proposed guidelines and numerically simulated under reversed cyclic loading sustained an average displacement corresponding to an IDR of 5.43%. These brace models could sustain 23 cumulative cycles before buckling locally and fracturing in the mid-length plastic hinge.
- The recommended design and detailing methodology is governed by the following:
    - Adequate detailing of the paddle-gusset plate connection in order to ensure that the flexural demands taking place in the paddle or gusset plate occur away from the SHG connection. This can be achieved through a paddle-gusset connection as shown in Fig. 3b-e or by respecting the $2t_g$ offset from the ends of the HSS tube.
    - Material grade investigated in this study is the ASTM A1085 grade which is comparable to the Canadian CSA G40.20/21 grade. Utilizing a different steel grade (e.g., ASTM A500B/C) should be carried out after proper consideration.

## Data Availability Statement

Some or all data, models, or code that support the findings of this study are available from the corresponding author upon reasonable request. (e.g., Python scripts, Abaqus subroutines, testing data, material properties, geometric properties of models).

## Acknowledgments

The authors would like to thank DPHV Structural Consultants, Constructions Proco, ADF Group Inc., and Atlas Tube for their technical and financial support, as well as the Natural Sciences and Engineering Research Council of Canada (NSERC) and the Fonds de recherche du Québec – Nature et technologies (FRQ-NT). The finite element computations were conducted on the supercomputer Graham cluster, which is managed by Calcul Québec and Compute Canada. Operation of the supercomputer is funded by the Canada Foundation for Innovation (CFI), NanoQuébec, RMGA and the Fonds de recherche du Québec - Nature et technologies (FRQ-NT).

## References

Afifi M, Tremblay R, and Rogers C.A. 2019. Evaluation of the behaviour and constructability of Slotted-Hidden-Gap HSS brace connections", 12th Canadian Conference on Earthquake Engineering, Quebec, Canada.

Afifi M, Tremblay R, and Rogers C.A. 2020. Slotted-Hidden-Gap (SHG) brace connections for square hollow structural sections for seismic applications ", 17th World Conference on Earthquake Engineering, Sendai, Japan.

Afifi, M., Moreau, R., Tremblay, R., and Rogers, C.A. 2021. Evaluation of the Slotted-Hidden-Gap (SHG) Connection for Square HSS Brace Members. Journal of Constructional Steel Research 179: 106548.

Afifi, M., Tremblay, R., and Rogers, C.A. 2022. Numerical & Experimental Investigation of Slotted-Hidden-Gap (SHG) Connection for Square HSS Brace Members. Journal of Constructional Steel Research 192: 107234.

AIJ. 2002. Recommendations for the design and fabrication of tubular truss structures in steel. Architectural Institute of Japan, Tokyo, Japan.

ANSI/AISC 341. 2016. Seismic provisions for structural steel buildings. American Institute of Steel Construction: Chicago, IL, USA.

ANSI/AISC 360. 2016. Specification for structural steel buildings. American Institute of Steel Construction: Chicago, IL, USA.

ASTM. 2015. Standard Specification for Cold-Formed Welded Carbon Steel Hollow Structural Sections (HSS). A1085/A1085M-15. American Society for Testing and Materials: West Conshohocken, PA, USA.

Autodesk, Inc. 2019. AutoCAD.

CSA. 2019 CSA S16-19, Design of Steel Structures. Canadian Standards Association (CSA), Toronto, ON, Canada.

Cheng JJR, Kulak GL, Khoo HA. 1998: Strength of slotted tubular tension members. Canadian Journal of Civil Engineering, 25(6), 982-991.

Dassault Systèmes Simulia Corp. 2014. Abaqus. Providence, RI, USA

EN. Eurocode 8. 2014. Design of structures for earthquake resistance. European Committee for Standardaization.

Fell BV, Kanvinde AM, Deierlein GG, Myers AT, Fu X. 2006: Buckling and Fracture of Concentric Braces Under Inelastic Cyclic Loading. Steel Tips Series. Structural Steel Education Council, Moraga, CA.

Fell BV, Kanvinde AM, Deierlein GG, and Myers AT. 2009. Experimental Investigation of Inelastic Cyclic Buckling and Fracture of Steel Braces. Journal of Structural Engineering. 135:1-19

GB 50017.2017, Standard for design of steel structures. Ministry of Housing and Urban-Rural Development of People's Republic of China.

Haddad M, Tremblay R. 2006: Influence of Connection Design on the Inelastic Seismic Response of HSS Steel Bracing Members. Proc. of the 11th Int. Symp. and IIW Int. Conf. on Tubular Structures, Quebec City, QC, Canada, 639-646.

Koval, I. 2018. Accounting for cold working and residual stress effects on the axial strength of HSS bracing members. M.Sc. Thesis, Département des génies civil, géologique et des mines, École Polytechnique de Montréal, Montréal.

Lutz, M. 1996 Programming Python, O'Reilly & Associates, Inc.

Martinez-Saucedo, G., Packer, J. A., and Willibald, S. 2006. Parametric finite element study of slotted end connections to circular hollow sections. Engineering Structures 28: 1956-1971.

Martinez-Saucedo, G. 2007. Slotted End Connections to Hollow Sections. Department of Civil Engineering, University of Toronto, Toronto, Canada.

Martinez-Saucedo, G., Packer, J. A., and Christopoulos, C. 2008a. Gusset Plate Connections to Circular Hollow Section Braces under Inelastic Cyclic Loading. Journal of Structural Engineering 134 (7): 1252-1258.

Martinez-Saucedo, G., Packer, J. A., and Tremblay, R. 2008b. Seismic response of circular hollow section braces with slotted end connections. Tubular Structures XII, Proceedings of Tubular Structures XII, Shanghai, China.

MIT Abaqus documentation 2017. Scripting parametric studies. < https://abaqus-docs.mit.edu/2017/English/SIMACAEANLRefMap/simaanl-c-scriptparstudies.htm#simaanl-c-scriptparstudies-t-bibliography-c1__simaanl-c-usb-ref-lutz2>. Accessed 15 Dec. 2020.

Mitsui, Y., Kurobane, Y., and Endoh, K. 1985. Experimental study on ultimate strength and deformation capacity of welded tube-to-through gusset plate joints. Journal of Structural Engineering, Japan Society of Civil Engineers, 31 (B): 145-156.

Moreau R, Tremblay R, Rogers CA 2014: Evaluation of the Modified-Hidden-Gap Connection for Square HSS Brace Members. Research Report, Dept. of Civil Eng., McGill University, Montreal, QC, Canada.

Okazaki, T., Lignos, D. G., Hikino, T., and Kajiwara, K. 2013. Dynamic Response of a Chevron Concentrically Braced Frame. Journal of Structural Engineering 139 (4): 515-525.

Packer, J. A., Chiew, S. P., Tremblay, R., and Martinez-Saucedo, G. 2010. Effect of material properties on hollow section performance. Proceedings of the Institution of Civil Engineers Structures and Buildings 163 (SB6): 375-390.

Sabelli R., Roeder CW, Hajjar JF. 2013: NEHRP Seismic Design Technical Brief No. 8-Seismic design of steel special concentrically braced frame systems: A guide for practicing engineers. Report no. NIST GCR 13-917-24, National Institute of Standards and Technology, Gaithersburg, MD.

Tremblay, R., Haddad, M., Martinez, G., Richard, J., and Moffat, K. 2008. Inelastic Cyclic Testing of Large Size Steel Bracing Members. The 14th World Conference on Earthquake Engineering, October 12-17, Beijing, China.

Willibald S, Packer JA, Martinez-Saucedo G. 2006: Behaviour of gusset plate connections to ends of round and elliptical hollow structural section members. Canadian Journal of Civil Engineering, 33(4), 373-383.

Yang, F., Mahin SA. 2005: Limiting Net Section Fracture in Slotted Tube Braces. Steel Tips Series. Structural Steel Education Council, Moraga, CA.

Zhao RG, Huang RF, Khoo HA, Cheng JJR. 2008: Experimental study on slotted rectangular and square hollow structural section (HSS) tension connections. Canadian Journal of Civil Engineering, 35(11), 1318-1330.

**Table 1** – Summary of research on SHG HSS brace connection

| Research Program | Objective | Methodology | Specimens | Main Findings |
|---|---|---|---|---|
| Mitsui et al., 1985<br>AIJ, 2002 | Eliminate need to reinforce connections at net area | Experimental: Monotonic Tension | 1 conventional + 5 extended plate configurations<br>CHS 140×3.5mm STK41 | -All braces attained measure yield resistance on gross area ($T_{exp}>A_gF_y$)<br>-Limit gap to 6mm, plate flap depth not to exceed 10 times HSS thickness |
| Martinez-Saucedo et al., 2006-2008 | Utilizing extended plate configuration for seismic applications | FEA and Experimental: Monotonic tension & cyclic loading | 1 conventional + 2 SHG<br>CHS 168 × 6.35mm<br>ASTM A500 B/C | -Increase weld length ($L_w$) to eliminate shear lag effects, and allow higher gap lengths to allow for reasonable fabrication tolerances<br>-Increase notch plate flap depth to limit bowing (rotation) in the plate |
| Packer et al., 2010 | Evaluate seismic performance of HSS braces fabricated from different hot & cold formed grades | Experimental: Reversed cyclic loading | 4 SHG Configurations<br>CHS 168.3×8-12.7mm<br>ASTM A500 Grade C + EN 10210 grade S355J2H | -Specimens showed extensive yielding with no fractures at connection<br>-Braces attained ultimate load of $1.3A_gF_y$ & IDR 2.5% |
| Okazaki et al., 2013 | Examine dynamic response of CBF chevron bracing connected using SHG connection | Experimental: Reversed cyclic loading | 1 bay 1 storey chevron CBF subject to earthquake motion with SHG Braces HSS 75×75×3.2mm STKR 400 | -No damage in the plate, brace ends or welds<br>-Braces fractured at plastic hinges |
| Moreau et al., 2014 | Determine minimum weld overlap length required | FEA and Experimental: Monotonic tension & cyclic loading | 5 conventional + 10 SHG<br>HSS152×152×9.5 + HSS203×203×13<br>CSA G40.20-21 350W Class C | -Net section fracture of conventional connection and SHG braces yielded on gross area<br>-Weld overlap length of 5% of weld length is sufficient to develop yield resistance of SHG conn.<br>-SHG brace achieved interstorey drift ratio of 3.14% |
| Afifi et al., 2019-2021 | Provide design and detailing rules for SHG Connection | FEA and Experimental: Monotonic tension & cyclic loading | 4 SHG Configurations<br>HSS 254×254×13<br>ASTM A1085 | -Understanding load transfer mechanism of SHG connection and influence of different elements<br>-SHG braces with no weld extension beyond the HSS slot ruptured on their net area<br>-Utilizing equivalent smaller-sized longer length welds attained higher tensile loads and larger brace strains before failure<br>-SHG models with 20mm overlap length survived an interstorey drift ratio of 5.29% |

**Table 2** – Parametric study base models

| # | HSS | $A_g$ (mm$^2$) | Weld Configuration A | | | Weld Configuration B | | |
|---|---|---|---|---|---|---|---|---|
| | | | $L_w$ (mm) | $D_w$ (mm) | $t_g$ (mm) | $L_w$ (mm) | $D_w$ (mm) | $t_g$ (mm) |
| 1 | 406×406×22 | 32,900 | 610 | 38 | 41 | 920 | 25 | 41 |
| 2 | 406×406×19 | 28,600 | 610 | 35 | 38 | 920 | 22 | 38 |
| 3 | 305×305×19 | 20,360 | 450 | 32 | 38 | 700 | 22 | 35 |
| 4 | 305×305×16 | 17,700 | 450 | 29 | 29 | 700 | 19 | 32 |
| 5 | 203×203×16 | 11,200 | 280 | 29 | 29 | 520 | 16 | 29 |
| 6 | 203×203×13 | 9,260 | 280 | 25 | 25 | 520 | 13 | 25 |
| 7 | 203×203×9.5 | 7,150 | 280 | 19 | 19 | 520 | 10 | 16 |
| 8 | 152×152×13 | 6,680 | 210 | 22 | 25 | 390 | 13 | 19 |
| 9 | 152×152×9.5 | 5,210 | 230 | 16 | 19 | 390 | 10 | 16 |
| 10 | 152×152×7.9 | 4,430 | 230 | 16 | 19 | 390 | 10 | 13 |
| 11 | 102×102×7.9 | 2,810 | 160 | 13 | 16 | 280 | 8 | 16 |
| 12 | 102×102×6.4 | 2,320 | 160 | 13 | 13 | 280 | 8 | 13 |
| 13 | 102×102×4.8 | 1,790 | 160 | 10 | 13 | 280 | 6 | 13 |
| 14 | 76×76×6.4 | 1,670 | 110 | 13 | 13 | 220 | 8 | 13 |
| 15 | 76×76×4.8 | 1,310 | 110 | 10 | 10 | 220 | 6 | 10 |

**Table 3** – Summary of minimum required weld overlap length for models with weld configuration A

| # | HSS | $A_g$ ($mm^2$) | $L_w$ (mm) | $D_w$ (mm) | $t_g$ (mm) | U | $A_{ne}$ ($mm^2$) | $L_{wg,\ min}$ (mm) | $L_{wg}/L_w$ | $L_{wg}/t_{slot}$ | $X_v$ |
|---|---|---|---|---|---|---|---|---|---|---|---|
| 1 | 406×406×22 | 32,900 | 610 | 38 | 41 | 0.88 | 27,233 | 40 | 6.6% | 0.91 | 1.10 |
| 2 | 406×406×19 | 28,600 | 610 | 35 | 38 | 0.87 | 23,519 | 40 | 6.6% | 0.98 | 1.18 |
| 3 | 305×305×19 | 20,360 | 450 | 32 | 38 | 0.88 | 16,539 | 30 | 6.7% | 0.73 | 0.90 |
| 4 | 305×305×16 | 17,700 | 450 | 29 | 29 | 0.87 | 14,514 | 30 | 6.7% | 0.94 | 1.14 |
| 5 | 203×203×16 | 11,200 | 280 | 29 | 29 | 0.87 | 8,859 | 20 | 7.1% | 0.63 | 0.82 |
| 6 | 203×203×13 | 9,260 | 280 | 25 | 25 | 0.86 | 7,352 | 20 | 7.1% | 0.71 | 0.90 |
| 7 | 203×203×9.5 | 7,150 | 280 | 19 | 19 | 0.86 | 5,788 | 20 | 7.1% | 0.91 | 1.12 |
| 8 | 152×152×13 | 6,680 | 210 | 22 | 25 | 0.88 | 5,253 | 17 | 8.1% | 0.61 | 0.91 |
| 9 | 152×152×9.5 | 5,210 | 230 | 16 | 19 | 0.89 | 4,265 | 17 | 7.4% | 0.77 | 0.94 |
| 10 | 152×152×7.9 | 4,430 | 230 | 16 | 19 | 0.89 | 3,633 | 17 | 7.4% | 0.77 | 1.10 |
| 11 | 102×102×7.9 | 2,810 | 160 | 13 | 16 | 0.90 | 2,259 | 13 | 7.8% | 0.66 | 0.82 |
| 12 | 102×102×6.4 | 2,320 | 160 | 13 | 13 | 0.90 | 1,904 | 13 | 7.8% | 0.78 | 0.95 |
| 13 | 102×102×4.8 | 1,790 | 160 | 10 | 13 | 0.90 | 1,473 | 12 | 7.5% | 0.75 | 0.91 |
| 14 | 76×76×6.4 | 1,670 | 110 | 13 | 13 | 0.89 | 1,304 | 10 | 9.1% | 0.63 | 0.82 |
| 15 | 76×76×4.8 | 1,310 | 110 | 10 | 10 | 0.88 | 1,043 | 10 | 7.3% | 0.77 | 0.97 |
| **Average** | | **10,226** | **288.7** | **21.3** | **23.1** | **0.88** | **8,329** | **20.4** | **7.3%** | **0.76** | **0.98** |

**Table 4** – Summary of minimum required weld overlap length for models with weld configuration B

| # | HSS | $A_g$ ($mm^2$) | $L_w$ (mm) | $D_w$ (mm) | $t_g$ (mm) | U | $A_{ne}$ ($mm^2$) | $L_{wg,\ min}$ (mm) | $L_{wg}/L_w$ | $L_{wg}/t_{slot}$ | $X_v$ |
|---|---|---|---|---|---|---|---|---|---|---|---|
| 1' | 406×406×22 | 32,900 | 920 | 25 | 41 | 0.95 | 29,399 | 40 | 4.3% | 0.91 | 1.02 |
| 2' | 406×406×19 | 28,600 | 920 | 22 | 38 | 0.95 | 25,682 | 40 | 4.3% | 0.98 | 1.09 |
| 3' | 305×305×19 | 20,360 | 700 | 22 | 35 | 0.96 | 18,152 | 30 | 4.3% | 0.79 | 0.89 |
| 4' | 305×305×16 | 17,700 | 700 | 19 | 32 | 0.95 | 15,758 | 30 | 4.3% | 0.86 | 0.96 |
| 5' | 203×203×16 | 11,200 | 520 | 16 | 29 | 0.98 | 9,979 | 25 | 4.8% | 0.78 | 0.89 |
| 6' | 203×203×13 | 9,260 | 520 | 13 | 25 | 0.97 | 8,292 | 23 | 4.4% | 0.82 | 0.92 |
| 7' | 203×203×9.5 | 7,150 | 520 | 10 | 16 | 0.97 | 6,584 | 20 | 3.8% | 1.05 | 1.14 |
| 8' | 152×152×13 | 6,680 | 390 | 13 | 19 | 0.98 | 5,999 | 20 | 5.4% | 0.95 | 1.06 |
| 9' | 152×152×9.5 | 5,210 | 390 | 10 | 16 | 0.97 | 4,704 | 18 | 4.6% | 0.95 | 1.05 |
| 10' | 152×152×7.9 | 4,430 | 390 | 10 | 13 | 0.97 | 4,052 | 15 | 3.8% | 0.94 | 1.02 |
| 11' | 102×102×7.9 | 2,810 | 280 | 8 | 16 | 0.99 | 2,485 | 15 | 5.4% | 0.79 | 0.89 |
| 12' | 102×102×6.4 | 2,320 | 280 | 8 | 13 | 0.98 | 2,073 | 13 | 4.6% | 0.81 | 0.91 |
| 13' | 102×102×4.8 | 1,790 | 280 | 6 | 13 | 0.98 | 1,604 | 12 | 4.6% | 0.81 | 0.91 |
| 14' | 76×76×6.4 | 1,670 | 220 | 8 | 13 | 0.99 | 1,451 | 10 | 4.6% | 0.63 | 0.77 |
| 15' | 76×76×4.8 | 1,310 | 220 | 6 | 10 | 0.99 | 1,173 | 10 | 4.1% | 0.77 | 0.86 |
| **Average** | | **10,226** | **483.3** | **13.0** | **21.9** | **0.97** | **9,159** | **21.5** | **4.5%** | **0.85** | **0.96** |

**Table 5** – Summary of models and the corresponding failure limits.

| # | HSS | $A_g$ ($mm^2$) | $T_y$ Gross Area Yielding (kN) | Weld Configuration A | | | Weld Configuration B | | |
|---|---|---|---|---|---|---|---|---|---|
| | | | | $A_{ne}$ ($mm^2$) | $T_r$ Net Section Fracture (kN) | $1-(T_r/T_y)$ | $A_{ne}$ ($mm^2$) | $T_r$ Net Section Fracture (kN) | $1-(T_r/T_y)$ |
| 1 | 406×406×22 | 32,900 | 14,147 | 27,233 | 11,710 | 17.2% | 29,399 | 12,642 | 10.6% |
| 2 | 406×406×19 | 28,600 | 12,298 | 23,519 | 10,113 | 17.8% | 25,682 | 11,043 | 10.2% |
| 3 | 305×305×19 | 20,360 | 8,755 | 16,539 | 7,112 | 18.8% | 18,152 | 7,805 | 10.8% |
| 4 | 305×305×16 | 17,700 | 7,611 | 14,514 | 6,241 | 18.0% | 15,758 | 6,776 | 11.0% |
| 5 | 203×203×16 | 11,200 | 4,816 | 8,859 | 3,809 | 20.9% | 9,979 | 4,291 | 10.9% |
| 6 | 203×203×13 | 9,260 | 3,982 | 7,352 | 3,161 | 20.6% | 8,292 | 3,566 | 10.4% |
| 7 | 203×203×9.5 | 7,150 | 3,075 | 5,788 | 2,489 | 19.0% | 6,584 | 2,831 | 7.9% |
| 8 | 152×152×13 | 6,680 | 2,872 | 5,253 | 2,259 | 21.4% | 5,999 | 2,579 | 10.2% |
| 9 | 152×152×9.5 | 5,210 | 2,240 | 4,265 | 1,834 | 18.1% | 4,704 | 2,023 | 9.7% |
| 10 | 152×152×7.9 | 4,430 | 1,905 | 3,633 | 1,562 | 18.0% | 4,052 | 1,742 | 8.5% |
| 11 | 102×102×7.9 | 2,810 | 1,208 | 2,259 | 971 | 19.6% | 2,485 | 1,068 | 11.6% |
| 12 | 102×102×6.4 | 2,320 | 998 | 1,904 | 819 | 17.9% | 2,073 | 891 | 10.7% |
| 13 | 102×102×4.8 | 1,790 | 770 | 1,473 | 633 | 17.7% | 1,604 | 690 | 10.4% |
| 14 | 76×76×6.4 | 1,670 | 718 | 1,304 | 561 | 21.9% | 1,451 | 624 | 13.1% |
| 15 | 76×76×4.8 | 1,310 | 563 | 1,043 | 448 | 20.4% | 1,173 | 505 | 10.4% |
| **Average** | | **10,226** | **4,397** | **8,329** | **3,582** | **18.1%** | **9,159** | **3,938** | **10.4%** |

**Table 6** – Comparison of weld overlap length calculated with proposed equations against past recommendations for different weld configurations.

| # | HSS | Weld Configuration A | | $L_{wg}$ (mm) | | | Weld Configuration B | | $L_{wg}$ (mm) | | |
|---|---|---|---|---|---|---|---|---|---|---|---|
| | | $L_w$ (mm) | $D_w$ (mm) | Proposed Equation | Moreau, 2014 | AIJ, 2002 | $L_w$ (mm) | $D_w$ (mm) | Proposed Equation | Moreau, 2014 | AIJ, 2002 |
| 1 | 406×406×22 | 610 | 38 | 47.6 | 30.5 | 76.0 | 920 | 25 | 46.6 | 46.0 | 76.0 |
| 2 | 406×406×19 | 610 | 35 | 44.3 | 30.5 | 70.0 | 920 | 22 | 44.6 | 46.0 | 70.0 |
| 3 | 305×305×19 | 450 | 32 | 37.3 | 22.5 | 70.0 | 700 | 22 | 34.4 | 35.0 | 64.0 |
| 4 | 305×305×16 | 450 | 29 | 33.9 | 22.5 | 52.0 | 700 | 19 | 32.9 | 35.0 | 58.0 |
| 5 | 203×203×16 | 280 | 29 | 35.3 | 14.0 | 52.0 | 520 | 16 | 28.4 | 26.0 | 52.0 |
| 6 | 203×203×13 | 280 | 25 | 23.1 | 14.0 | 44.0 | 520 | 13 | 25.2 | 26.0 | 44.0 |
| 7 | 203×203×9.5 | 280 | 19 | 22.5 | 14.0 | 32.0 | 520 | 10 | 20.7 | 26.0 | 26.0 |
| 8 | 152×152×13 | 210 | 22 | 21.9 | 10.5 | 44.0 | 390 | 13 | 19.6 | 19.5 | 32.0 |
| 9 | 152×152×9.5 | 230 | 16 | 18.7 | 11.5 | 32.0 | 390 | 10 | 17.2 | 19.5 | 26.0 |
| 10 | 152×152×7.9 | 230 | 16 | 18.0 | 11.5 | 32.0 | 390 | 10 | 14.6 | 19.5 | 20.0 |
| 11 | 102×102×7.9 | 160 | 13 | 15.3 | 8.0 | 26.0 | 280 | 8 | 16.8 | 14.0 | 26.0 |
| 12 | 102×102×6.4 | 160 | 13 | 13.1 | 8.0 | 20.0 | 280 | 8 | 14.4 | 14.0 | 20.0 |
| 13 | 102×102×4.8 | 160 | 10 | 13.1 | 8.0 | 20.0 | 280 | 6 | 14.4 | 14.0 | 20.0 |
| 14 | 76×76×6.4 | 110 | 13 | 12.5 | 5.5 | 20.0 | 220 | 8 | 14.0 | 11.0 | 20.0 |
| 15 | 76×76×4.8 | 110 | 10 | 10.4 | 5.5 | 14.0 | 220 | 6 | 11.7 | 11.0 | 14.0 |
| **Average** | | **288.7** | **21.3** | **24.5** | **14.4** | **40.3** | **483.3** | **13.1** | **23.7** | **24.2** | **37.9** |

**Table 7** – Geometric properties and probable resistances of braces modelled under reversed cyclic loading

| # | HSS | $A_g$ ($mm^2$) | $L_w$ (mm) | $D_w$ (mm) | $t_g$ (mm) | $L_{wg}$ (mm) | $d_{flap}$ (mm) | $T_{prob}$ (kN) | $C_u$ (kN) | $C_u$' (kN) | IDR (%) |
|---|---|---|---|---|---|---|---|---|---|---|---|
| 1 | HSS 305×305×16 | 17,700 | 460 | 29 | 32 | 33 | 50 | 8,142 | 5,908 | 1,628 | 5.29% |
| 2 | HSS254×254×13 | 11,800 | 390 | 22 | 25 | 28 | 44 | 5,428 | 3,940 | 1,086 | 5.61% |
| 3 | HSS127×127×6.4 | 2,960 | 180 | 13 | 16 | 15 | 25 | 1,362 | 557 | 272 | 5.39% |

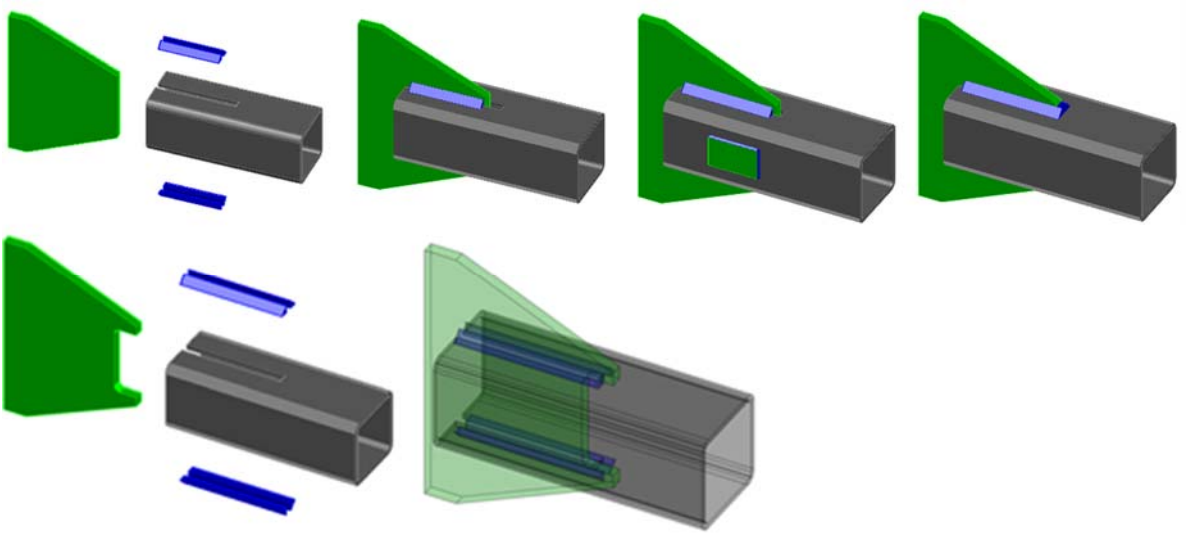

Fig. 1 – Left: Conventional HSS brace-to-plate connections: a) assembly of parts, b) unreinforced, c) with side-reinforcement plates, and d) with wrapped-around welds. Right: Slotted-Hidden-Gap (SHG) connection: e) assembly of parts and f) X-ray view.

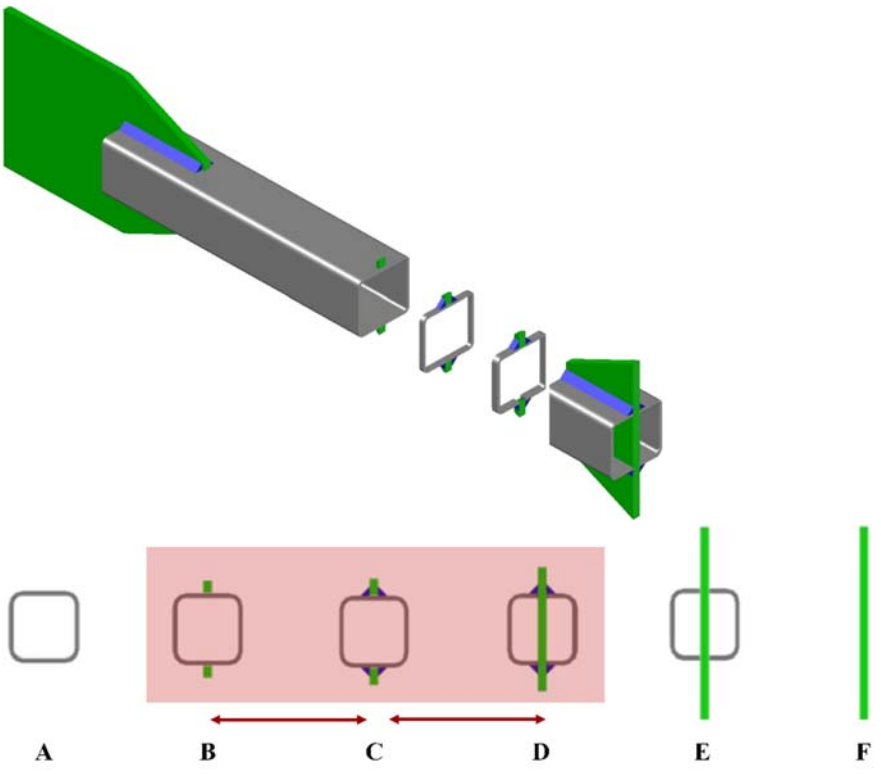


Fig. 2 – a) Diagram showing load path from HSS to plate in a SHG brace connection, and b) Cross sections along brace at principal locations.

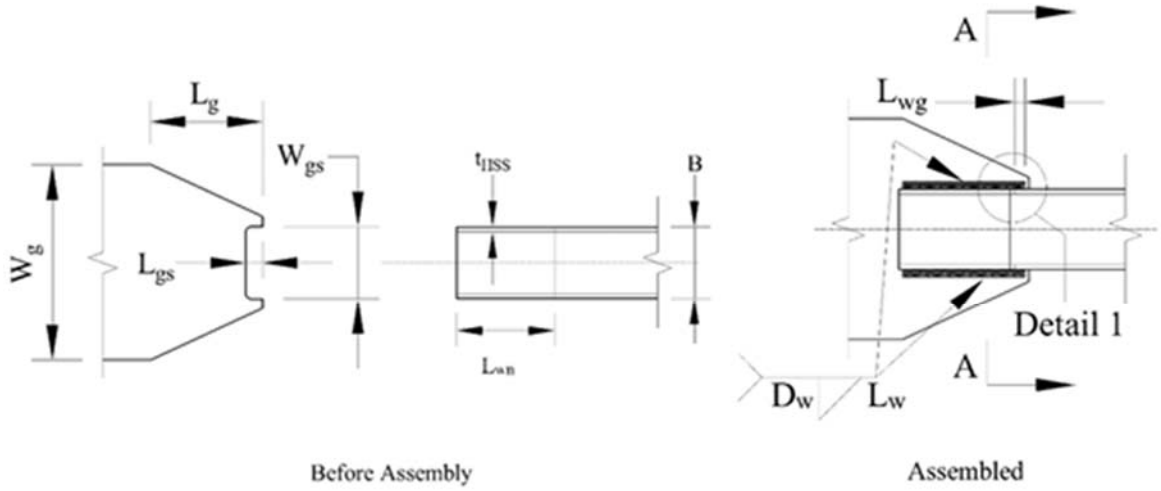


Before Assembly

Assembled

30

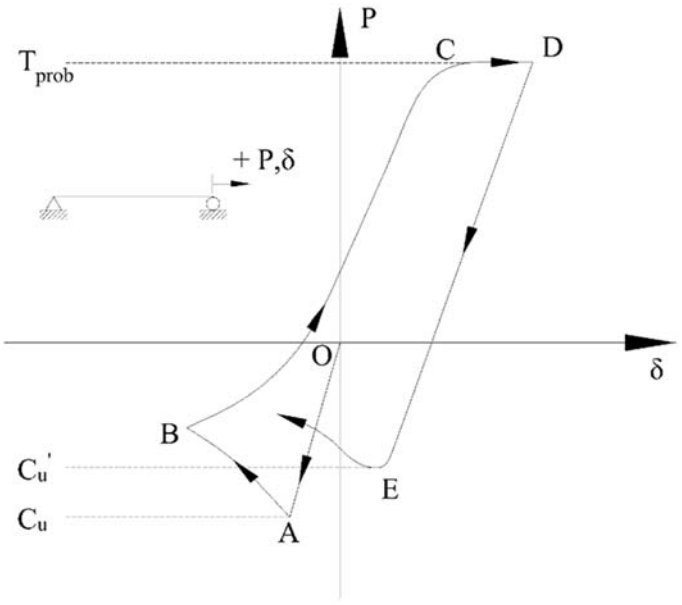


31

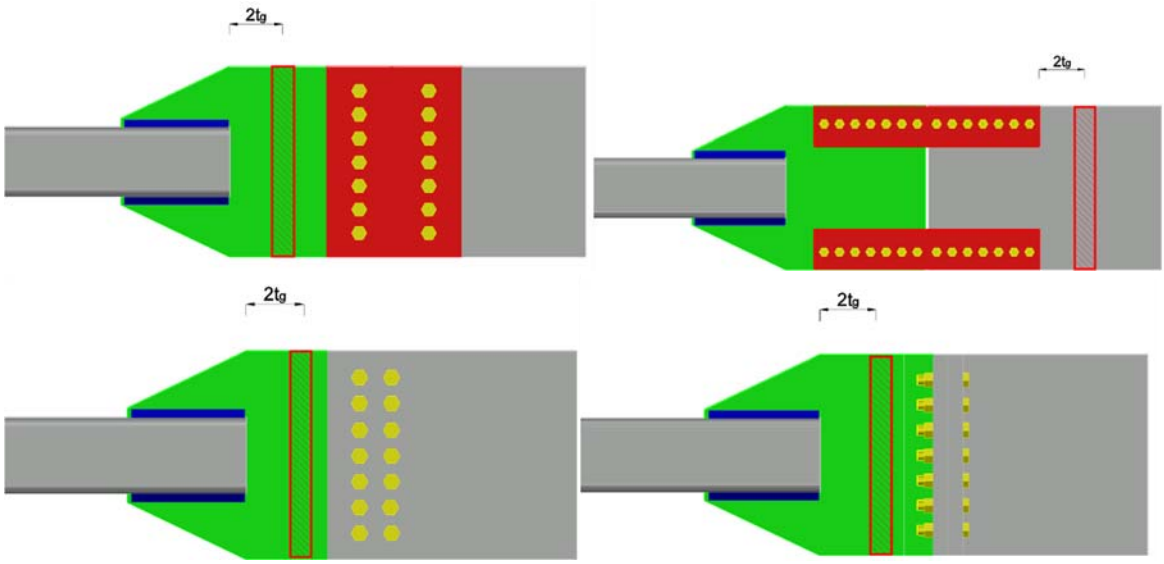


Fig. 3: a) Sample force-deformation hysteresis of a brace under cyclic axial loading, and paddle-gusset plate scenarios highlighting expected locations of plastic hinges; b) 2-Plates, c) 4-Angles, d) Splice plate, and e) T-stub.

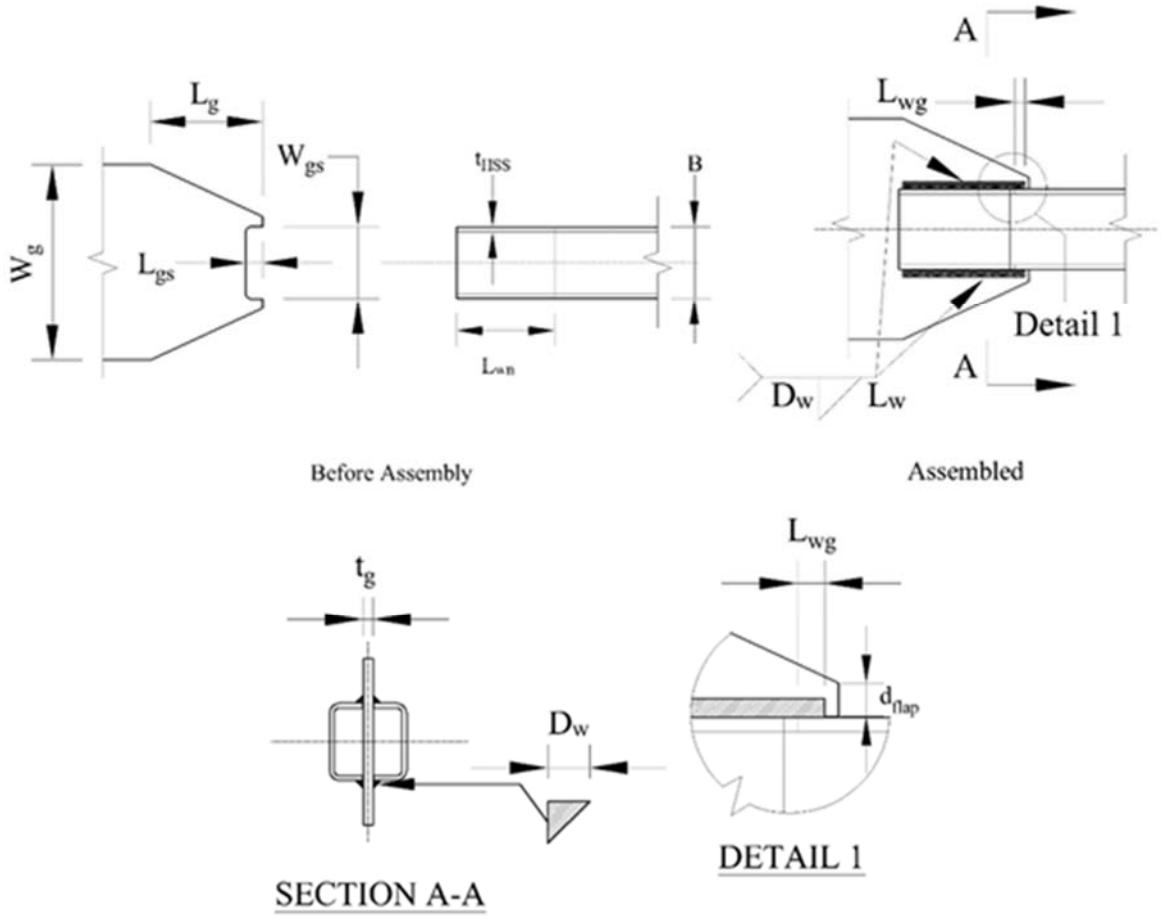


Fig. 4 – SHG Connection for square HSS braces showing geometric variables.

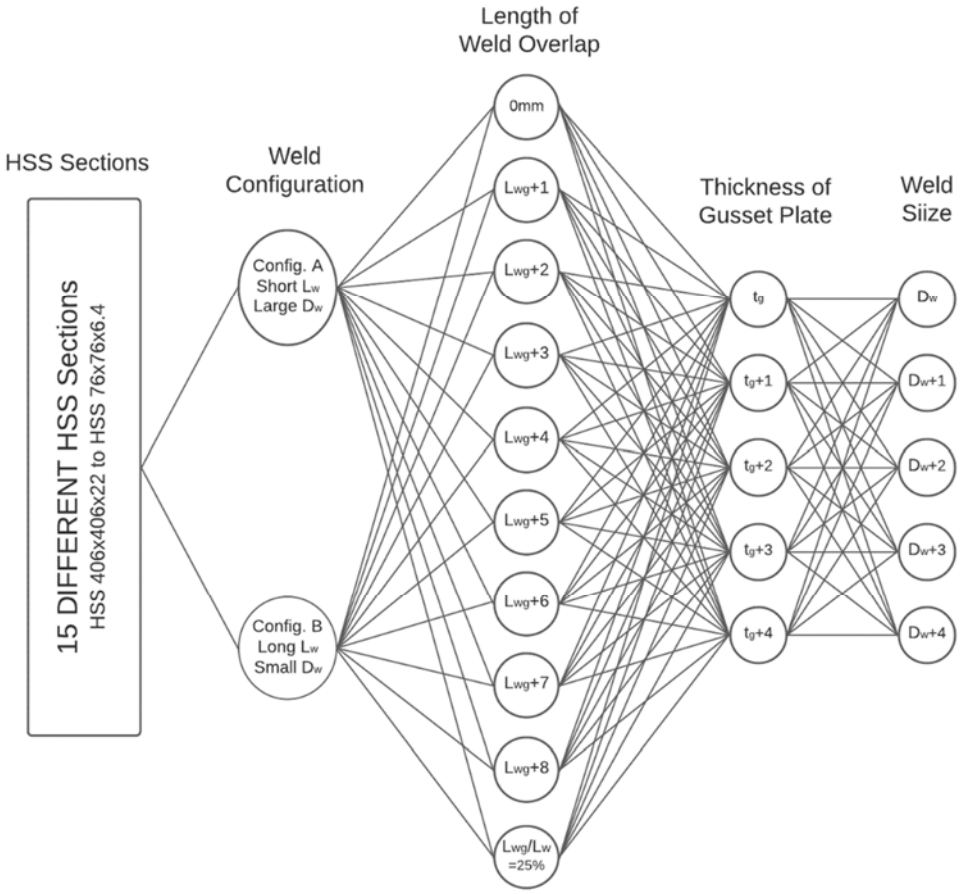


Fig. 5 – Overview of the numerical study parameters.

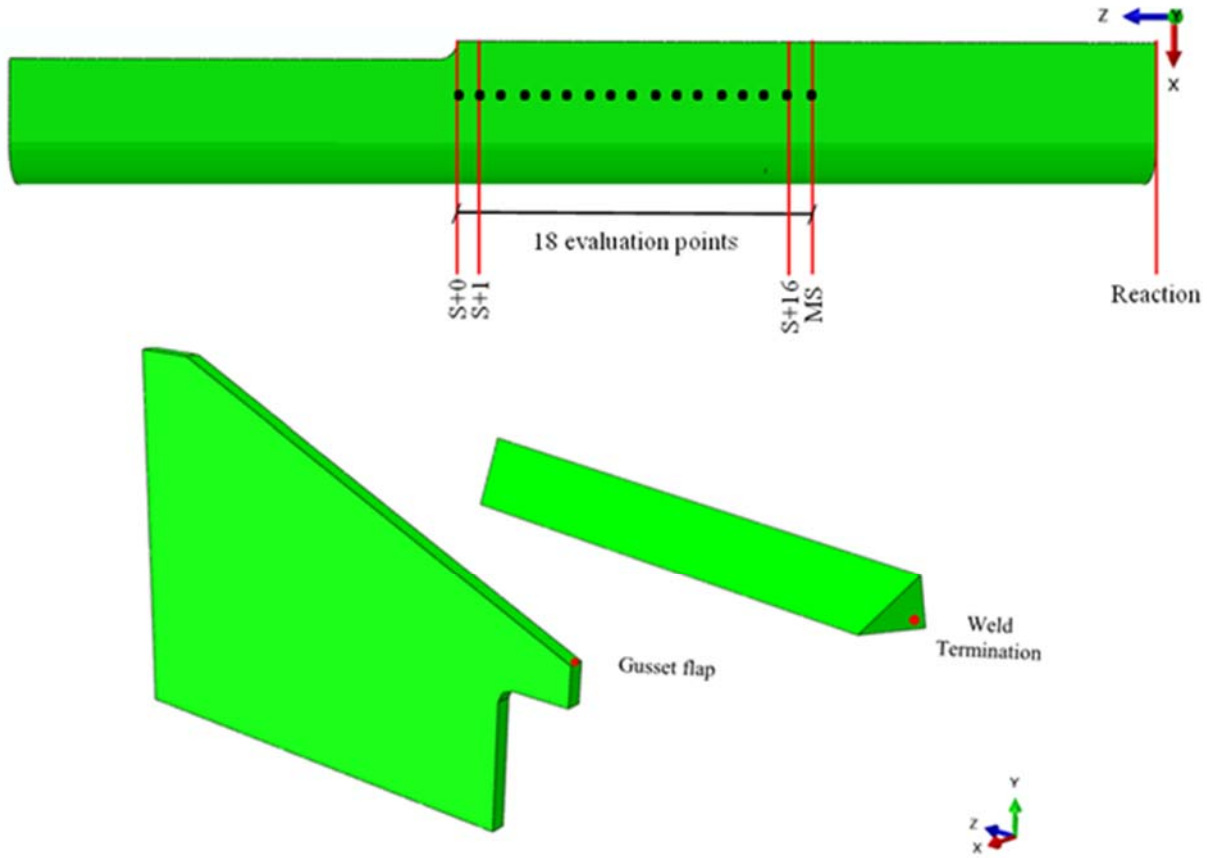


Fig. 6 – Locations of evaluation at the different elements of the SHG Connection.

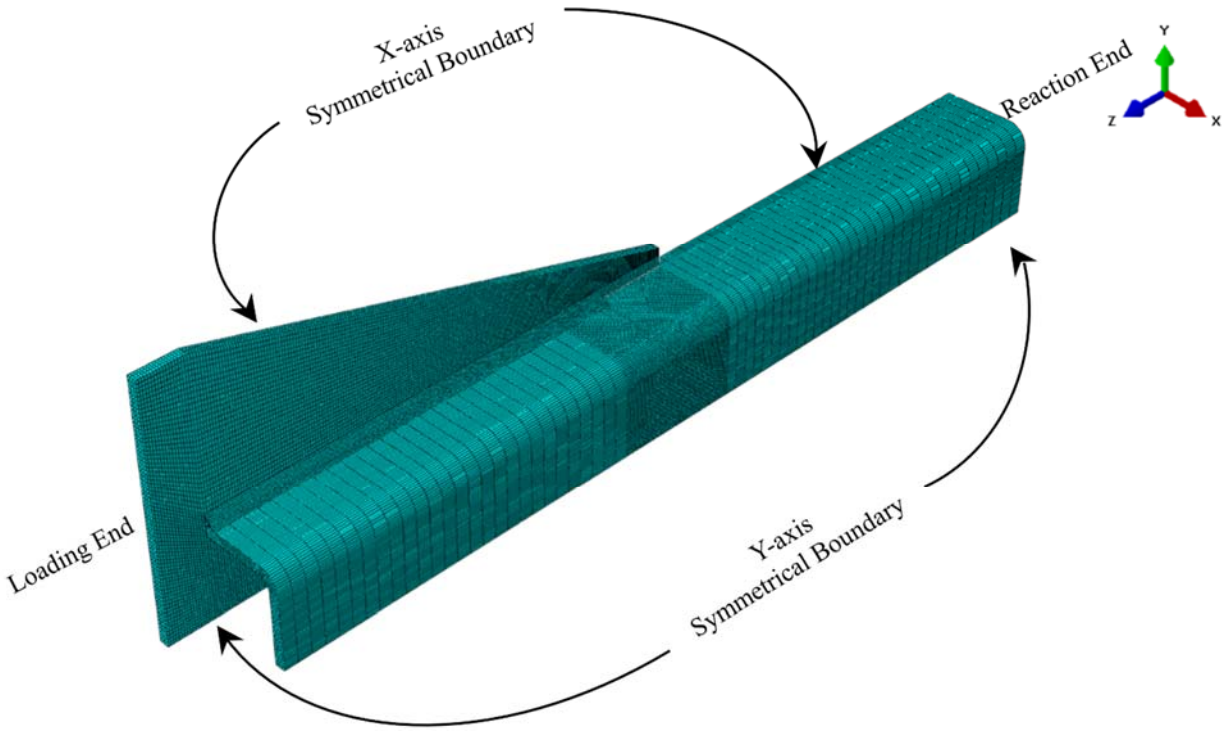


Fig. 7 - Typical FEM of SHG HSS brace connection showing boundary conditions.

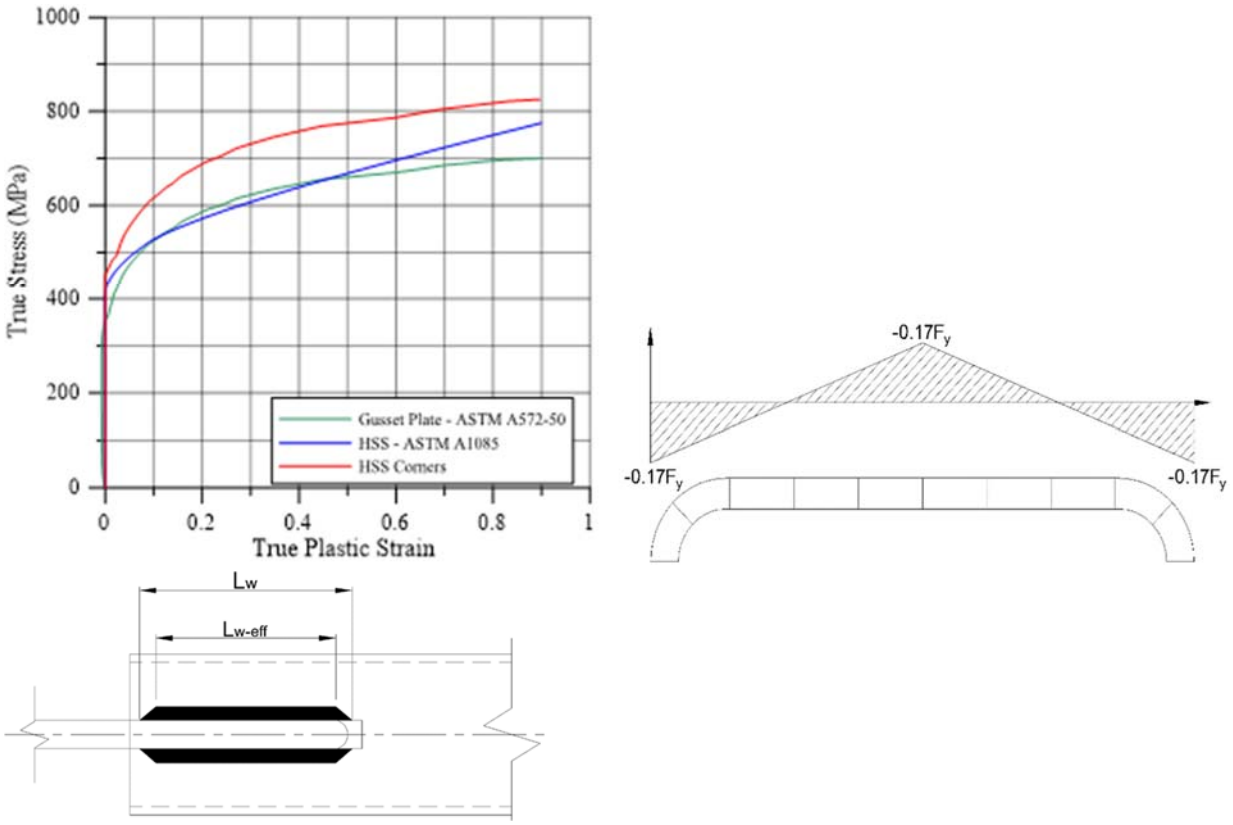


Fig. 8 – Features of FE models: a) True Stress vs. True Plastic Strain for HSS flats, HSS corners and Plate, b) Longitudinal Residual stress distribution, and c) Weld effective length as result of stepping.

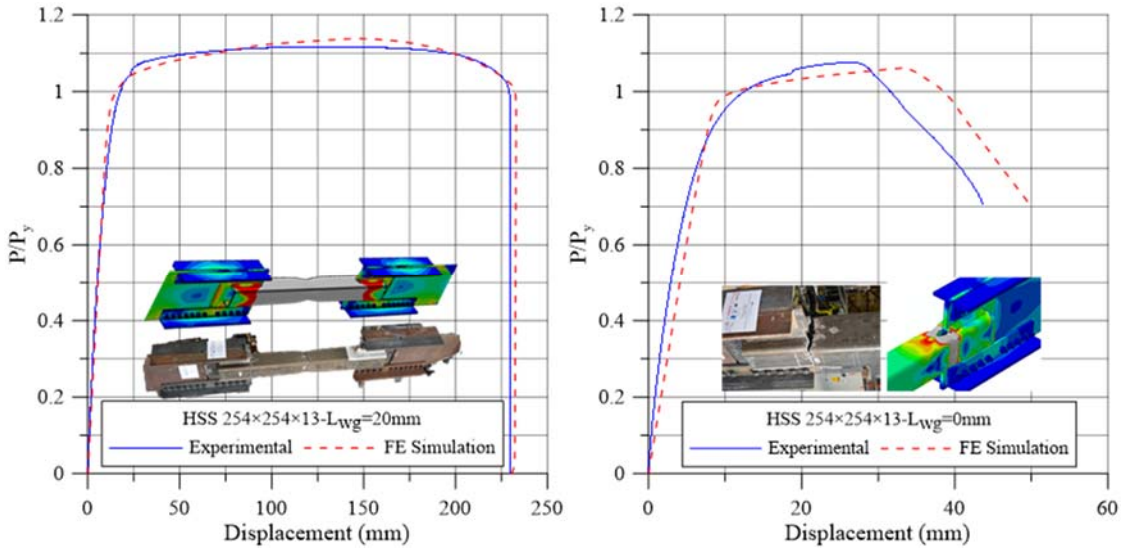


Fig. 9– Calibration of FE models of HSS 254×254×13 with a) $L_{wg}$=20mm and b) $L_{wg}$=0mm (weld configuration A)

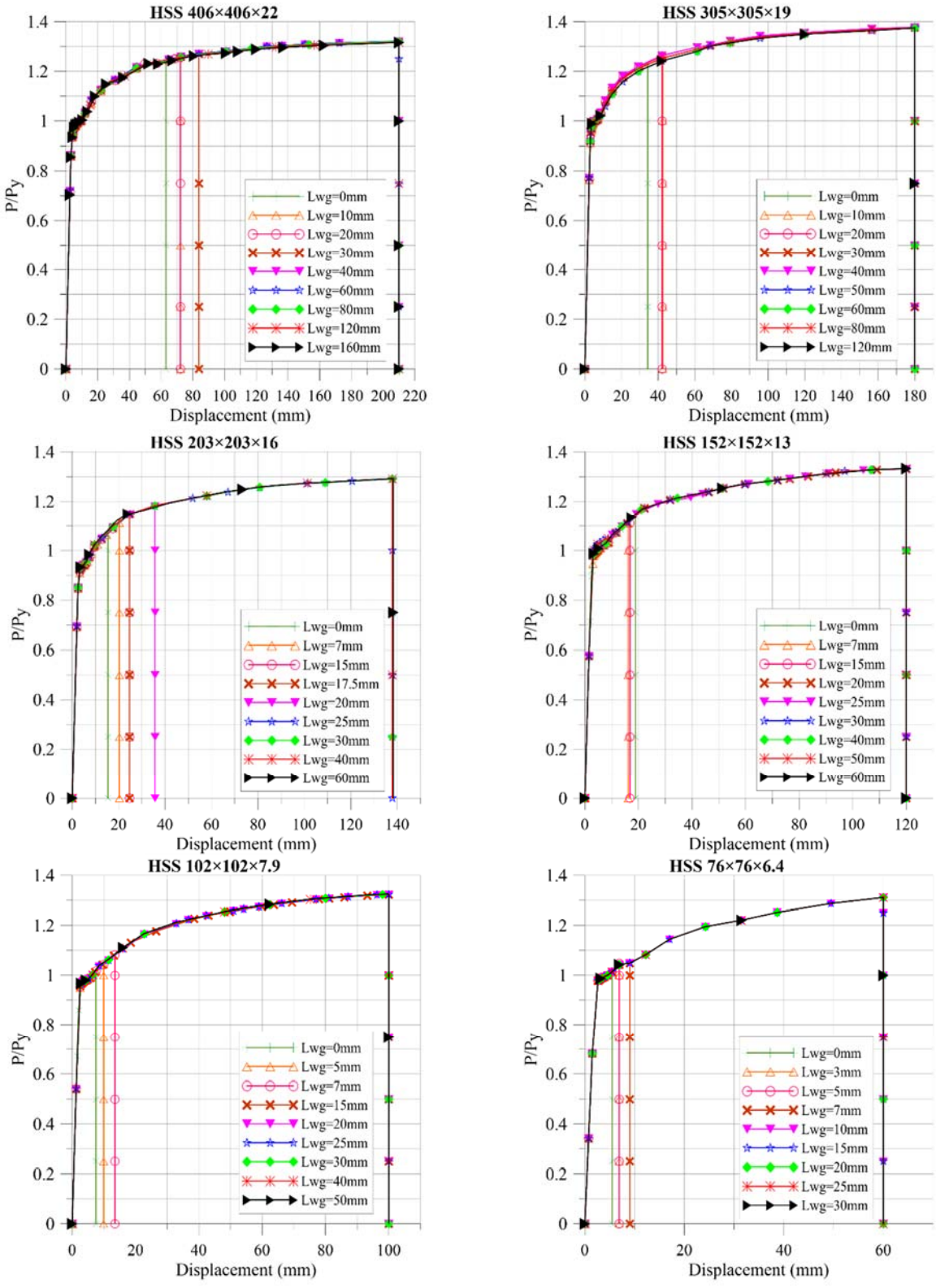


Fig.10 – Overall Load vs. displacement curves of SHG braces made with different HSS sizes and weld overlap lengths ($L_{wg}$) (weld configuration A).

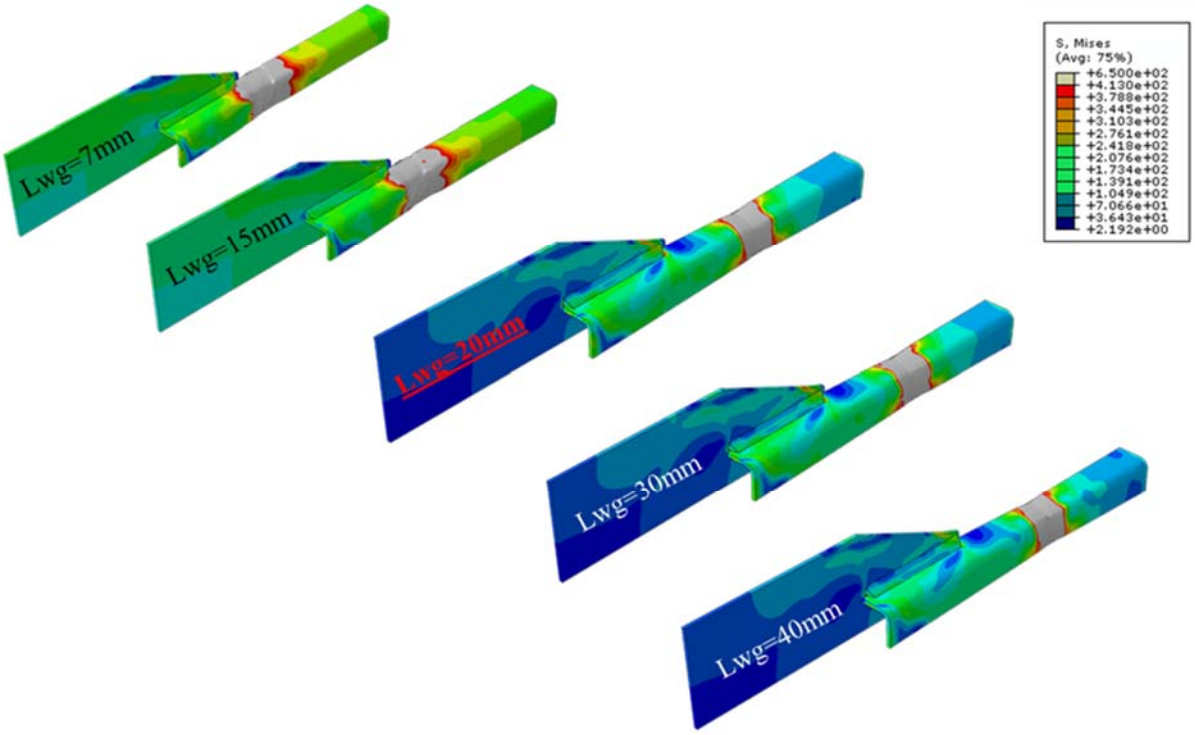


Fig. 11 – Variation of von Mises stresses and location of fracture for HSS203×203×13 with different weld overlap lengths (weld configuration A).

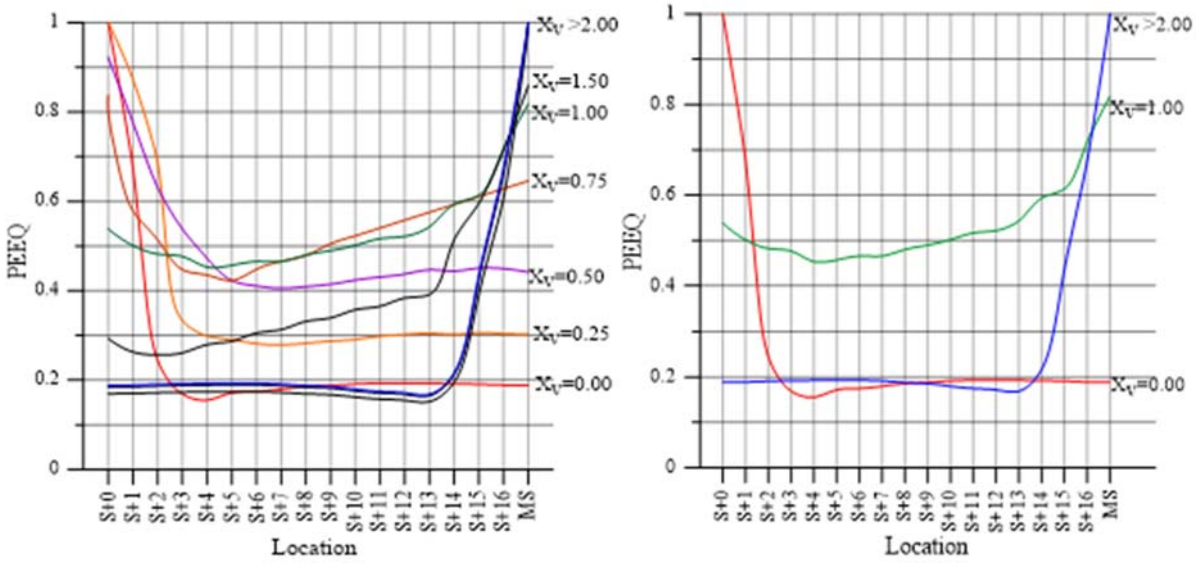


Fig. 12 – Variation of PEEQ at failure at different locations along HSS (Fig. 5) for all simulations: a) For all $X_v$ Values and b) Highlighting key $X_v$ Values.

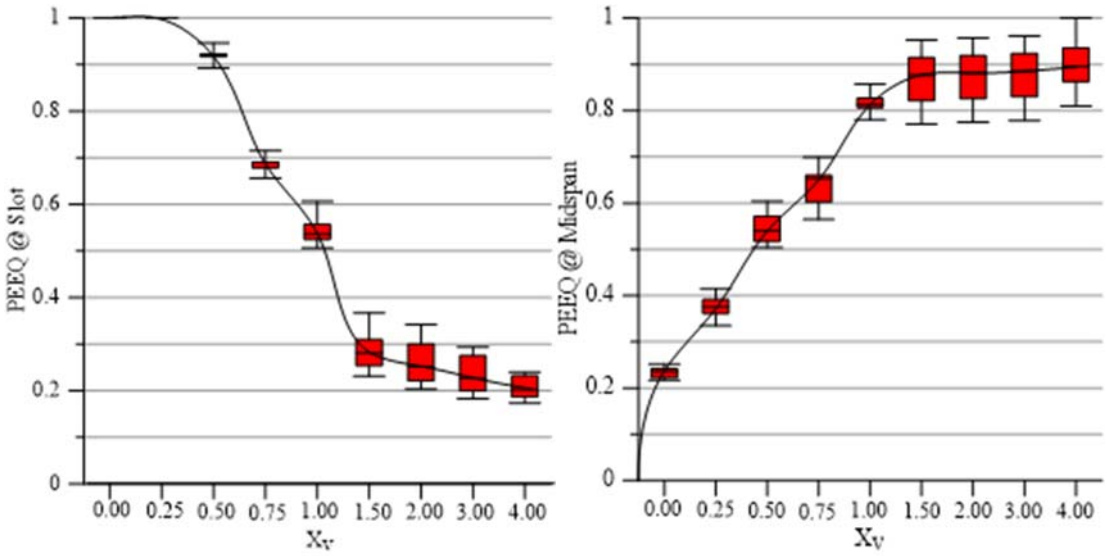


74

75 Fig. 13 – Variation of inelastic demands (PEEQ) vs. $X_v$ at: a) HSS slot and b) HSS mid-length.

76

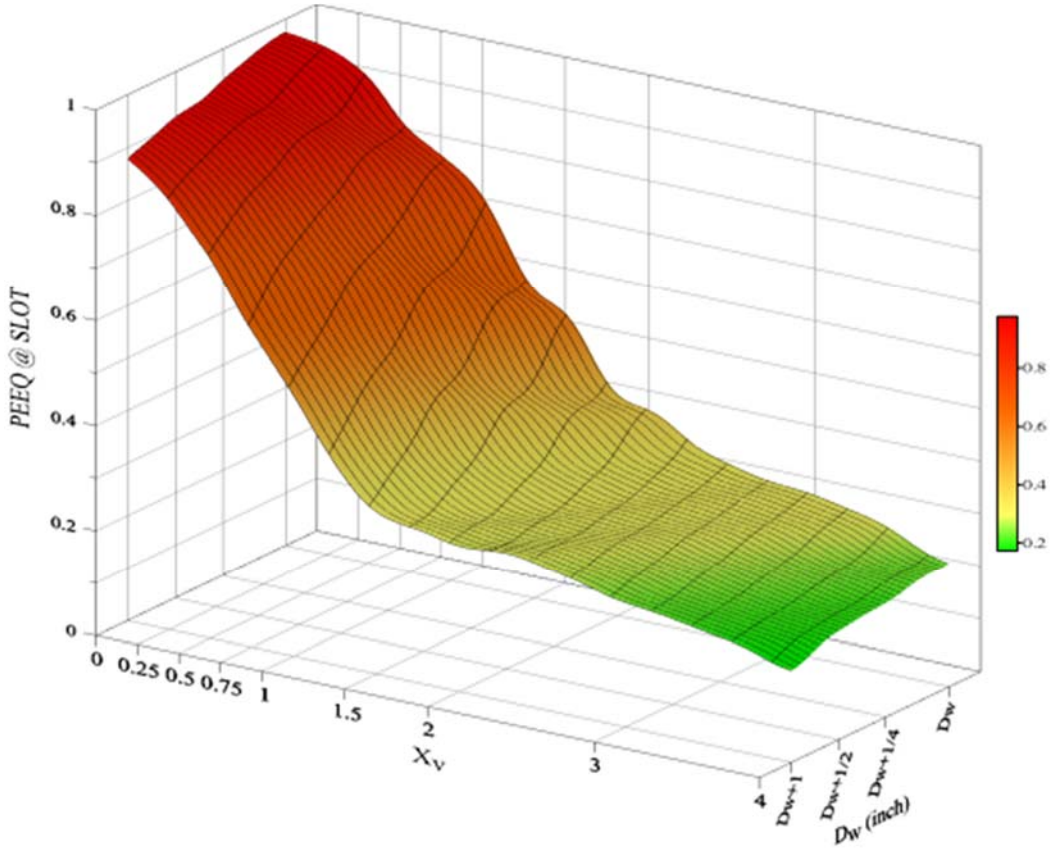


77

78 Fig. 14 – 3D Surface of inelastic demands (PEEQ) at slot with varying normalised ratio $X_v$ and
79 weld size $D_w$

80

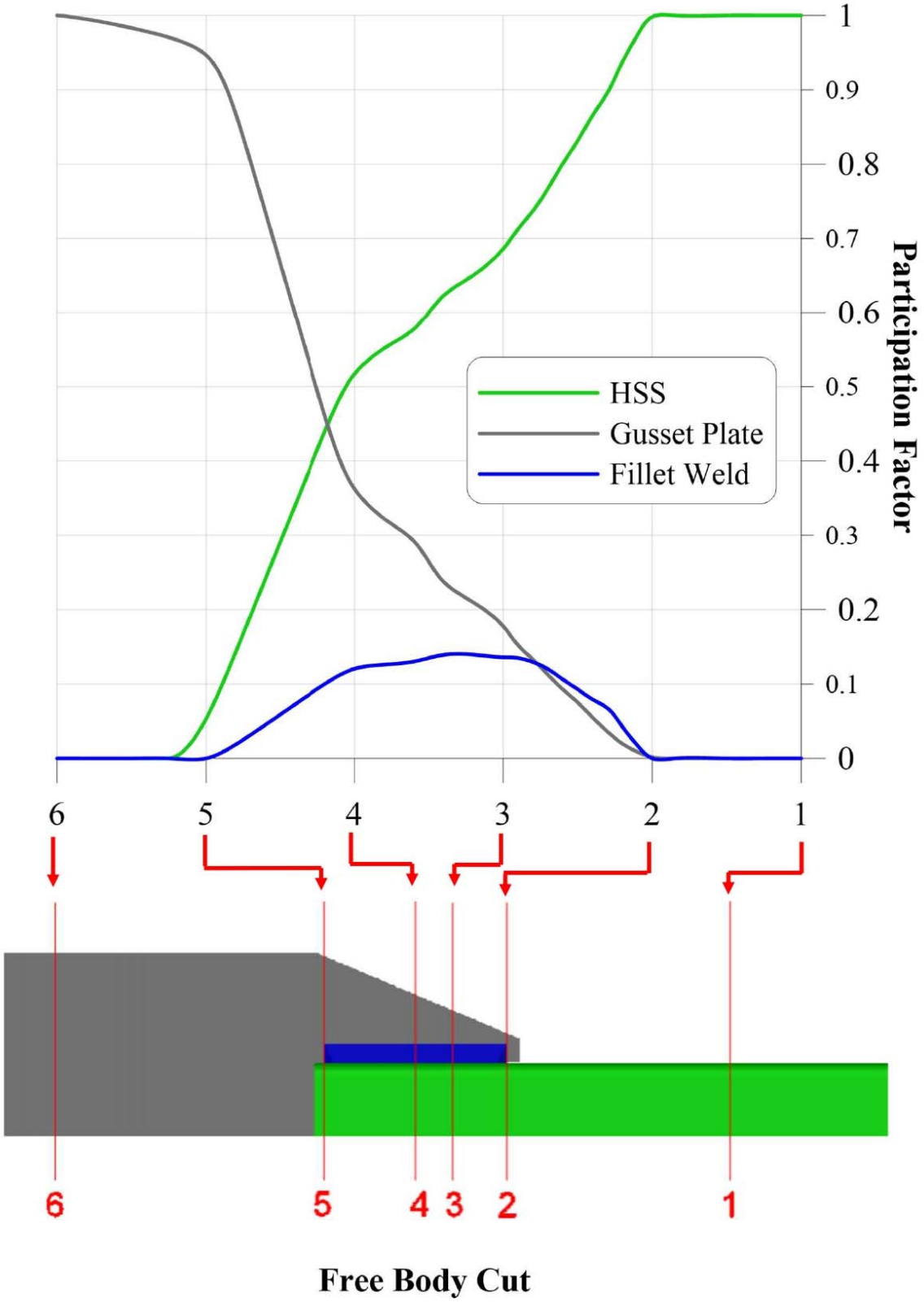
1
0.9
0.8
0.7
0.6
0.5
0.4
0.3
0.2
0.1
0
Participation Factor
HSS
Gusset Plate
Fillet Weld
6
5
4
3
2
1
6
5
4
3
2
1
Free Body Cut

81

82

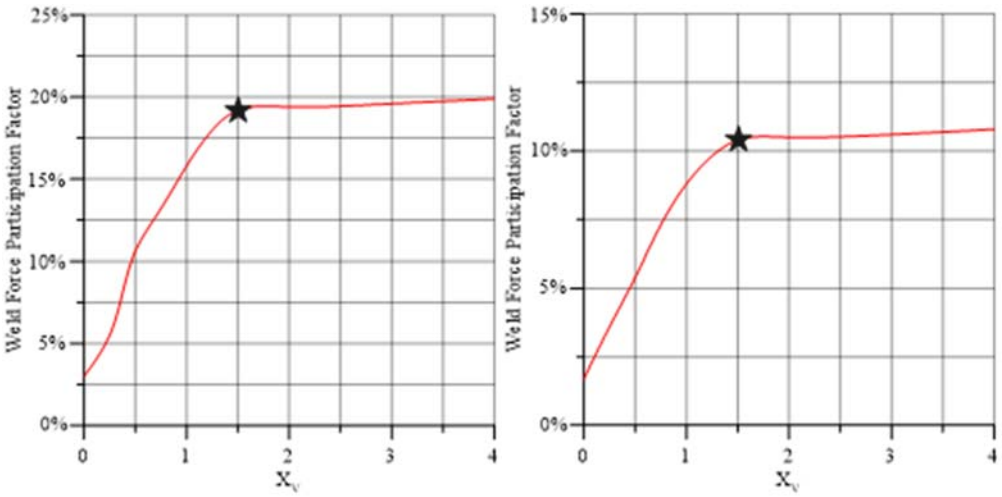


Fig. 15 – a) Free body cuts and force transfer for a typical SHG connection (Afifi et al., 2021) and Weld load participation factor (fillet weld) vs. $X_v$ for: b) Weld configuration A and c) Weld configuration B.

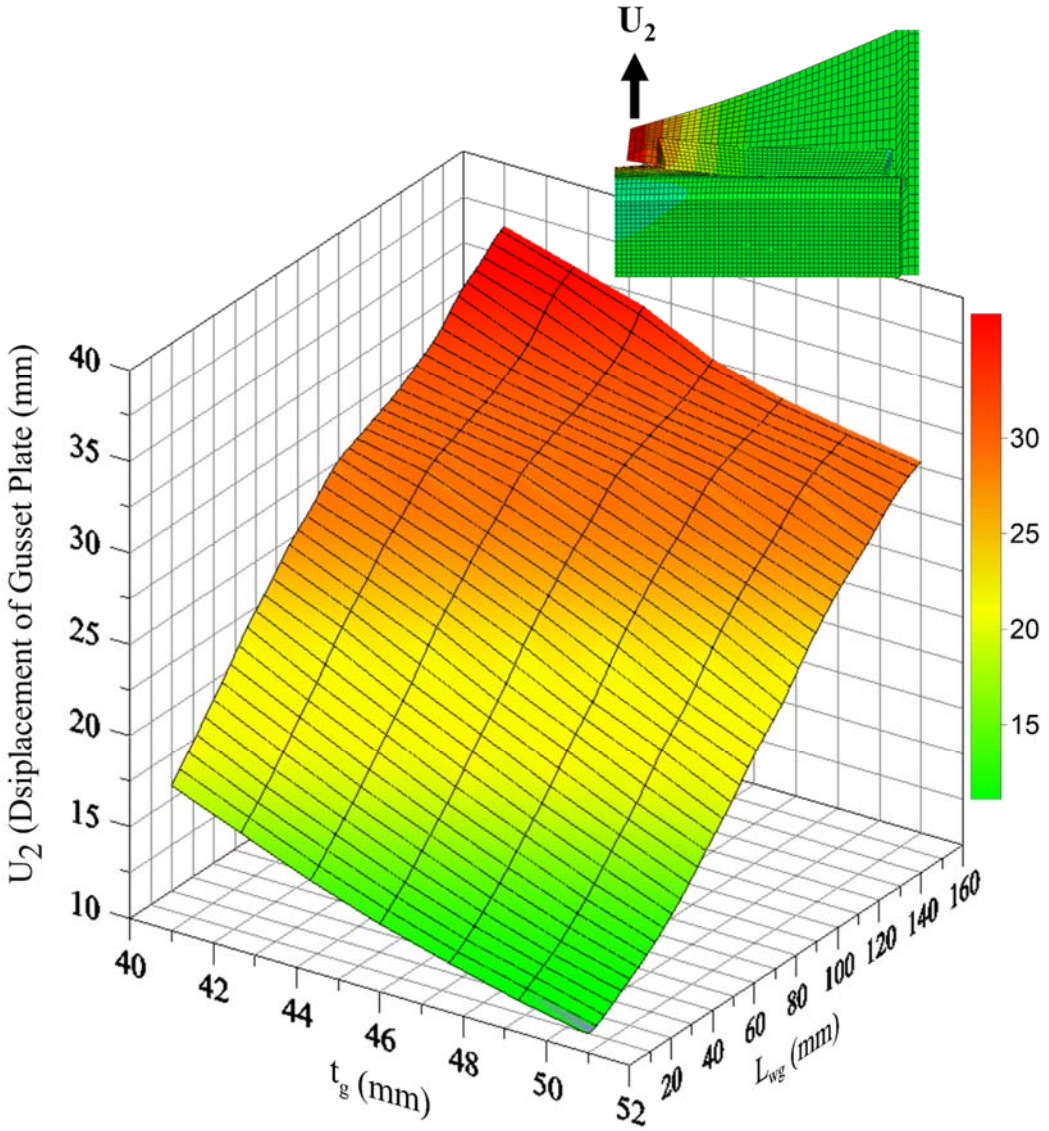


Fig. 16 - 3D Surface of $U_2$ displacement at plate with varying thickness ($t_g$) and weld overlap length ($L_{wg}$) for HSS 406×406×22

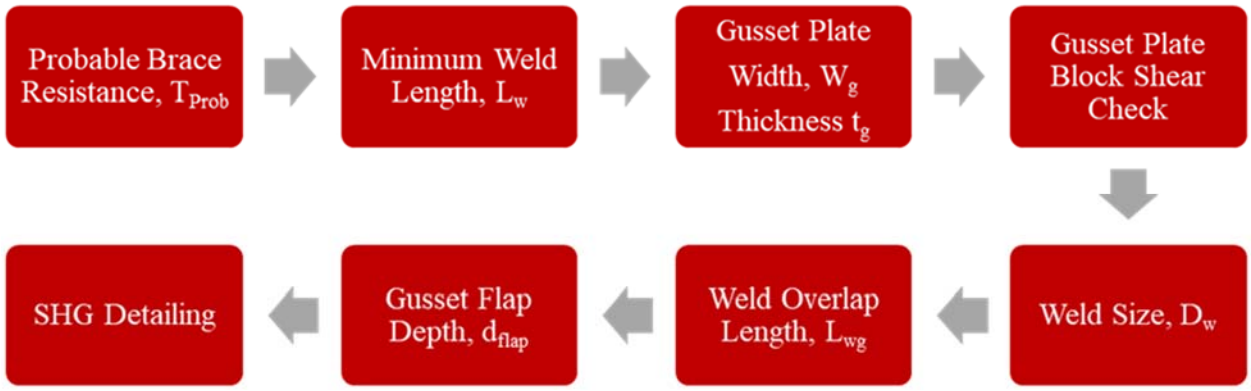


Fig. 17 – Proposed Design Methodology for SHG brace connections

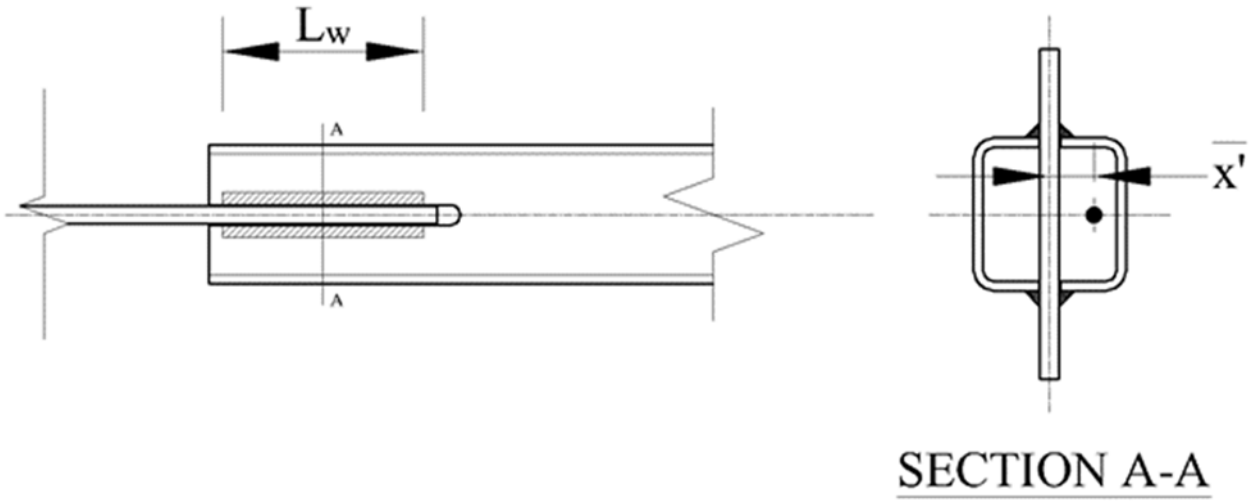


Fig. 18 – Shear lag variables

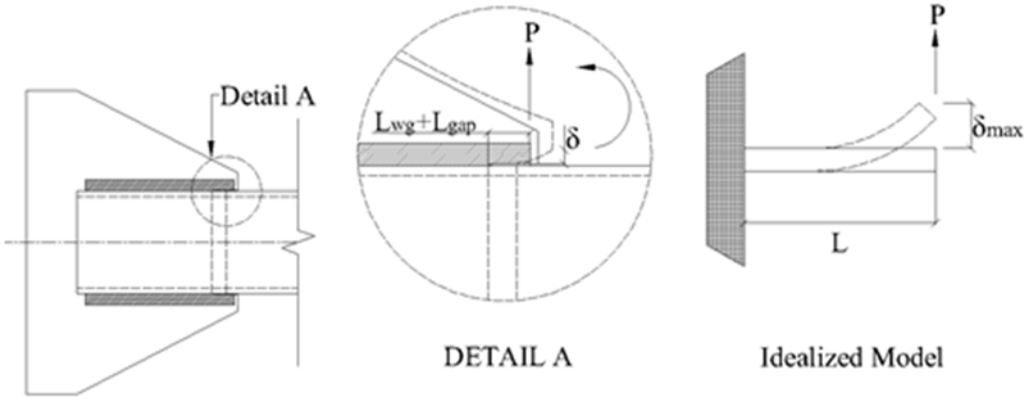


Fig. 19 – Paddle plate deflection and idealized model

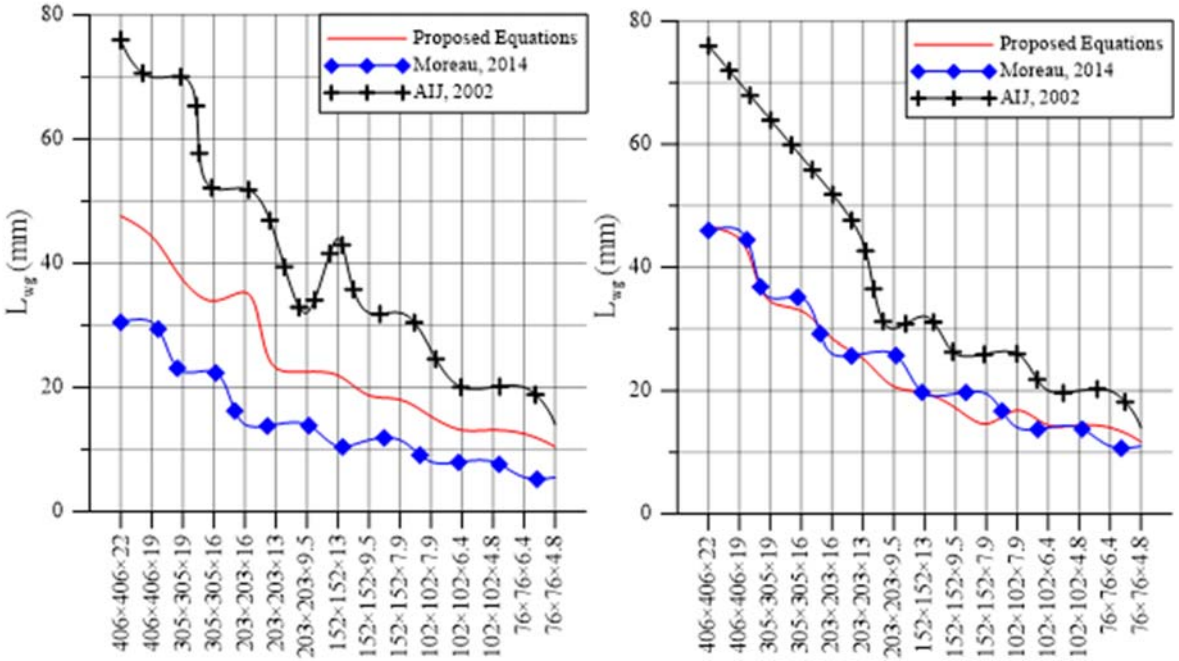


Fig. 20 – Weld Overlap length ($L_{wg}$) calculated with different recommendations for weld a) Configuration A and b) Configuration B.

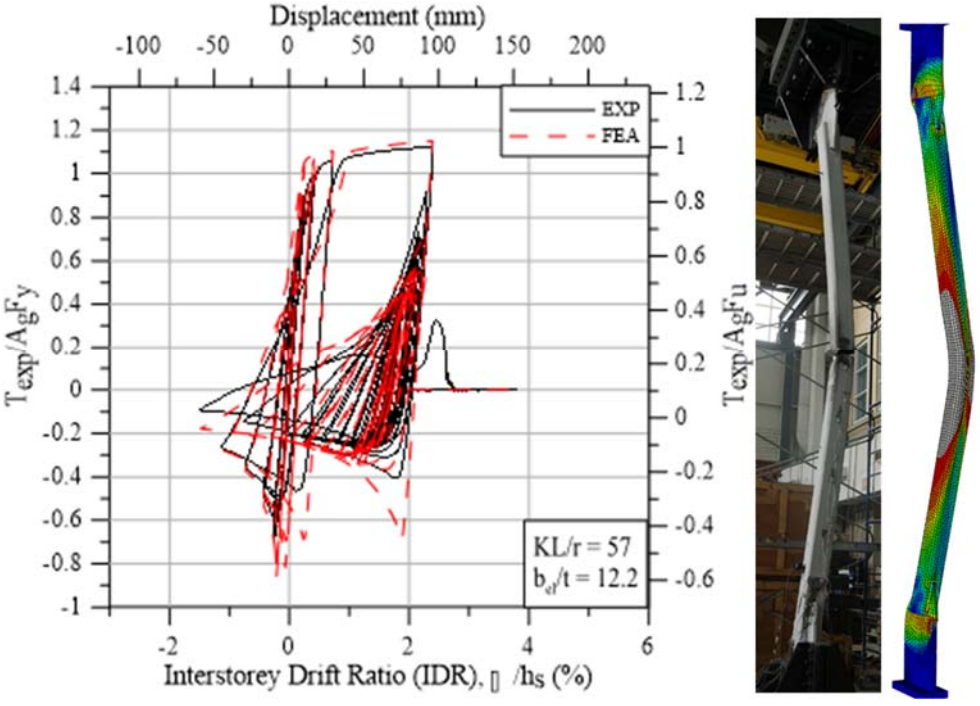


Fig. 21 – a) Comparison of the normalised overall load-displacement response obtained from the test by Moreau (Moreau et al., 2014) and the finite element analysis, and b) behaviour comparison of test specimen and FE model.

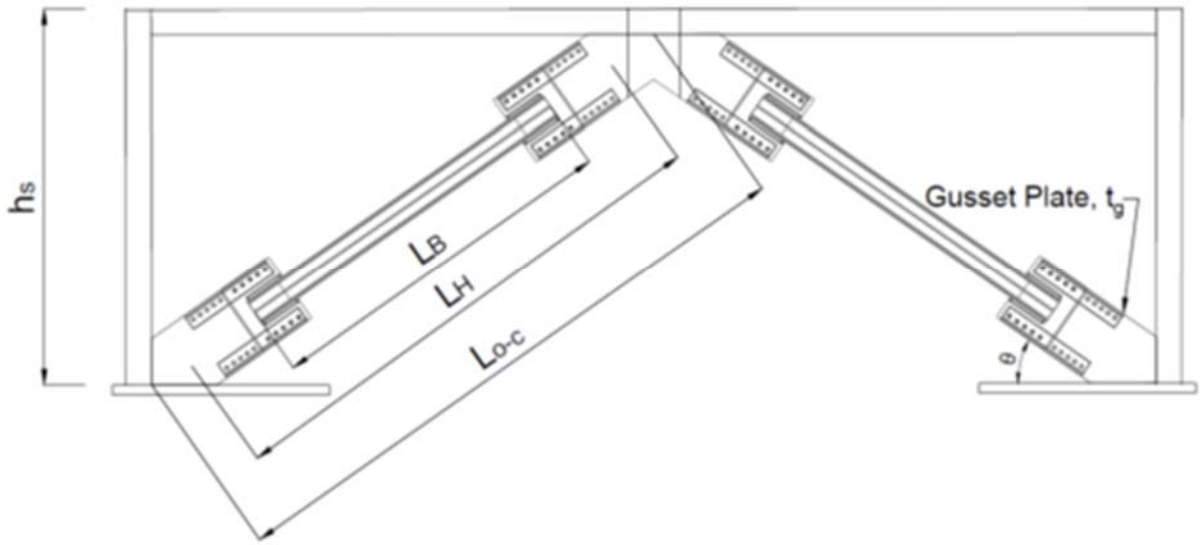


109

110 Fig. 22 - Schematic showing variables used to calculate storey drift based on brace axial
111 deformations in a typical chevron CBF.

112

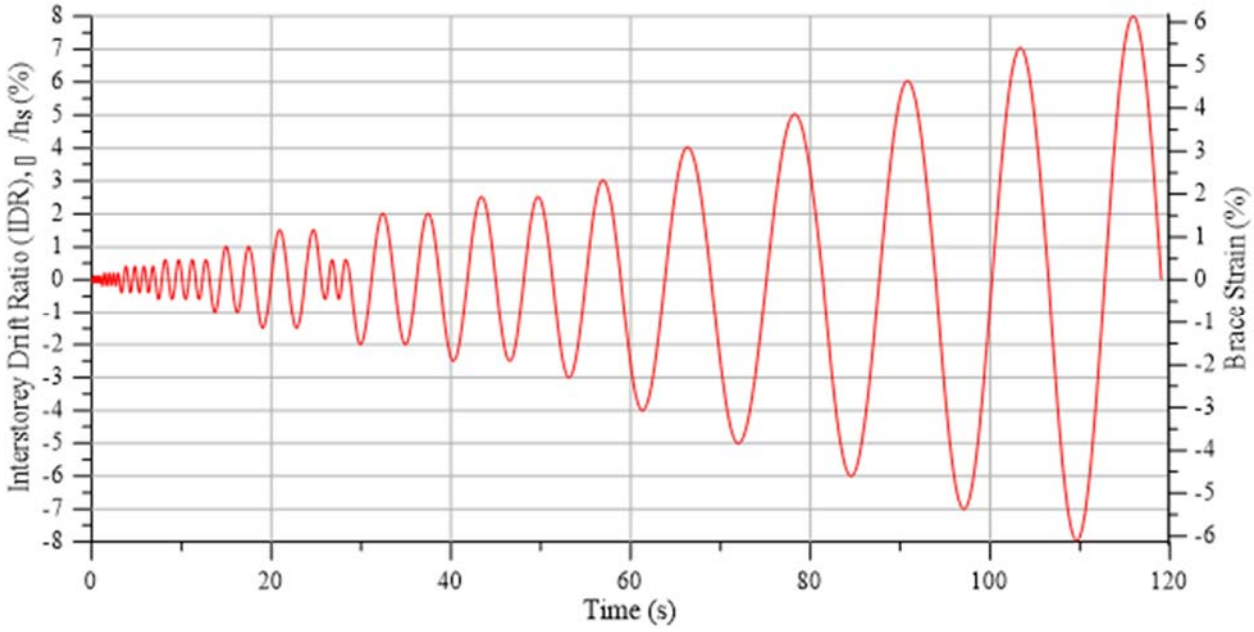


113

114 Fig. 23 – Reversed Cyclic Loading Protocol.

115

116

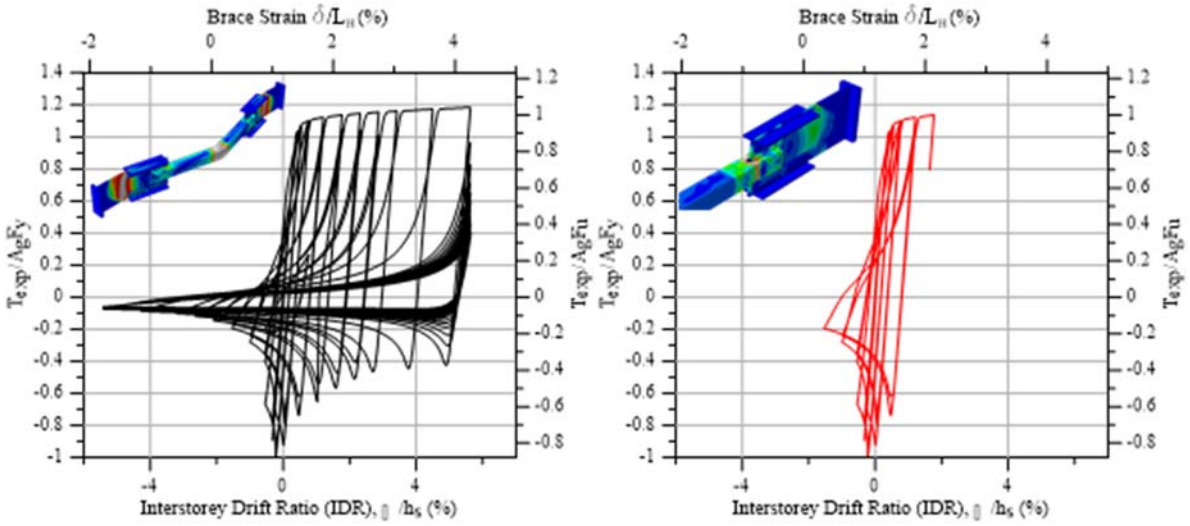


117

118

119 Fig. 24 – Normalised overall load-IDR for HSS 254×254×13 Brace with: a) SHG Connection
120 and b) Conventional Connection

121